EUROPEAN RESPIRATORY *journal*

FLAGSHIP SCIENTIFIC JOURNAL OF ERS

Early View

Original article

Decreased IDO1 Dependent Tryptophan Metabolism in Aged Lung during Influenza

Soo Jung Cho, Kyung Sook Hong, Edward Schenck, Stefi Lee, Rebecca Harris, Jianjun Yang, Augustine MK Choi, Heather Stout-Delgado

Please cite this article as: Cho SJ, Hong KS, Schenck E, *et al*. Decreased IDO1 Dependent Tryptophan Metabolism in Aged Lung during Influenza. *Eur Respir J* 2020; in press (https://doi.org/10.1183/13993003.00443-2020).

Decreased IDO1 Dependent Tryptophan Metabolism in Aged Lung during Influenza

Soo Jung Cho[1], Kyung Sook Hong[1], Edward Schenck[1], Stefi Lee[1], Rebecca Harris[1], Jianjun Yang[1], Augustine MK Choi[1], and Heather Stout-Delgado[1]

1: Department of Medicine, Pulmonary and Critical Care, Weill Cornell Medicine, New York, NY

Corresponding Author:

Heather Stout-Delgado

Pulmonary and Critical Care / Weill Cornell Medicine

1300 York Avenue, Box 96

New York, NY 10065

Phone : 212-746-4468

Fax : 212-746-7293

Email : hes2019@med.cornell.edu

Keywords: Influenza, Aging, Lung, Macrophage, Immunometabolism, Mitochondria, Kynurenine, Tryptophan Metabolism

Abstract

Influenza epidemics remain a leading cause of morbidity and mortality worldwide. In the current study, we investigated the impact of chronological aging on tryptophan metabolism in response to influenza infection. Examination of metabolites present in plasma collected from critically ill patients, identified tryptophan metabolism as an important metabolic pathway utilized specifically in response to influenza. Using a murine model of influenza infection to further these findings illustrated that there was decreased production of kynurenine in aged lung in an indoleamine-pyrrole 2,3-dioxygenase (IDO1)-dependent manner that was associated with increased inflammatory and diminished regulatory responses. Specifically, within the first seven days of influenza, there was a decrease in kynurenine pathway mediated metabolism of tryptophan, which resulted in a subsequent increase in ketone body catabolism in aged alveolar macrophages. Treatment of aged mice with mitoquinol, a mitochondrial targeted antioxidant, improved mitochondrial function and restored tryptophan metabolism. Taken together, our data provide additional evidence as to why older persons are more susceptible to influenza and suggest a possible therapeutic to improve immunometabolic responses in this population.

Introduction

Influenza epidemics still remain a leading cause of morbidity and mortality worldwide, with highest incidence of hospitalization and death occurring in persons >65 years of age [1]. ~~The plays an important role in regulating metabolic responses to influenza.~~ The kynurenine pathway (KP) of tryptophan metabolism is a highly regulated pathway utilized by the immune system to promote immunosuppression in response to excessive inflammation [2-9]. Kynurenine catabolites, such as quinolinate, are essential for the production of nicotinamide and NAD^+ as well as initiate involvement of type 2 T helper cell mediated resolution [7]. In response to heightened levels of cellular stress or energy usage, KP mediated oxidation of tryptophan can renew NAD^+ levels [10]. Tryptophan metabolism by the KP is initiated by indoleamine-pyrrole 2,3-dioxygenase (IDO1). IDO1 expression is tightly regulated by the immune system; specifically IDO1 is activated by pro-inflammatory cytokines and inhibited by regulatory, anti-inflammatory cytokines [2, 3, 11-15].

Despite the important role for KP mediated tryptophan metabolism in the initiation and regulation of immune response to influenza, little is known regarding the impact of aging and aging associated changes in mitochondrial stress on this metabolic pathway. In the current study, using plasma collected from critically ill patients, we show that tryptophan metabolism is an important metabolic pathway utilized specifically in response to influenza. Using a murine model of influenza infection to further these findings, our results illustrate decreased production of kynurenine in aged lung that was associated with increased inflammatory and diminished regulatory responses. Reduced IDO1 expression and activity in aged lung and alveolar macrophages corresponded with

changes in metabolic gene regulation and the initiation of alternative tryptophan metabolism pathways. Our findings demonstrated that decreased IDO expression was associated with dysregulated mitochondrial gene expression and heightened generation of reactive oxygen species. Treatment of aged mice with mitoquinol, a mitochondrial targeted antioxidant, improved mitochondrial function and restored KP mediated metabolism of tryptophan in alveolar macrophages and resulted in decreased inflammatory cytokine production and cellular recruitment to the aged lung.

Methods

Detailed methods are provided in the Supplementary Material.

Study approval and subjects

This study is an analysis of prospectively collected data from 39 subjects recruited from an ICU cohort from New York Presbyterian Hospital-Weill Cornell Medical Center (NYP-WCMC, IRB:1405015116). Protocols for recruitment, data collection, and sample processing have been described previously [16-20].

Mouse model of influenza

Animal experiments were performed in accordance with the animal guidelines of the Institutional Animal Care and Use Committee at Weill Cornell Medicine (IACUC: 2016-0059). Young (2 months) and aged (18 months) male and female BALB/c mice were purchased from the National Institute on Aging rodent facility (Charles River Laboratories). Influenza viral stock (material #: 10100374, batch #: 4XP170531, EID_{50}

per ml: $10^{10.3}$) was purchased from Charles River (Norwich, CT). Mice were anesthetized with isoflurane prior to intranasal instillation with 12.5 PFU of influenza (50μL volume in PBS). Mice received a 100μL volume of PBS or 10-50μg dose of mitoquinol (Cayman Chemical) intraperitoneally starting at day 3 post influenza. Starting at day 0, mice received a daily intraperitoneal injection containing PBS or BMS-986205 (200μM) (Selleck Chemicals).

Statistics

Statistical analysis was performed using Prism (GraphPad, La Jolla, CA). All samples were independent and contained the same sample size for analysis. P-values <0.05 were considered significant.

Results

Increased Tryptophan Metabolism in Response to Influenza Infection.

Using a principal component analysis to provide a high-level overview of the dataset, illustrated limited clustering of metabolites in plasma collected from control, influenza A/B positive patients, and patients with other viral infections (OVI) (**Figure 1A,** patient demographics and PCR confirmed microbiology results **Table 1**). Focusing on specific biochemical and pathway changes illustrated a distinct metabolic increase in several metabolic pathways, including tryptophan metabolism, that occurred in patients during the course of influenza infection (**Figure 1A-B**). When compared to influenza A/B samples, there was significantly elevated levels of tryptophan and serotonin present in

the plasma of patients with OVI (**Figure 1C-D**). In contrast, there was a significant increase in kynurenine and kynurenate present in plasma from the influenza A/B groups when compared to control, with significantly higher levels of kynurenate in influenza A/B positive patients (**Figure 1E-F**). To provide more insight, we evaluated kynurenine levels in plasma samples based on influenza severity (i.e. mild versus severe influenza). Severe influenza was defined as a positive influenza test result combined with acute respiratory distress syndrome (ARDS) requiring intubation. While patients with mild symptoms during influenza exhibited an age-associated trend in kynurenine expression, patients that exhibited severe influenza with ARDS had decreasing kynurenine and increasing tryptophan as they age (**Supplemental Figure 1A**). While these metabolites were also elevated in the OVI, the levels did not reach statistical significance, suggesting that influenza A/B infections cause the strongest inflammatory response. The further breakdown products quinolinate and xanthurenate were also examined, with significantly increased levels of quinolinate present in influenza A/B positive patients (**Figure 1G-H**).

Tryptophan Metabolism is Altered in Aged Lung during Influenza Infection.

In response to influenza, there was cellular infiltration in both young adult (2 months of age) and aged adult (18-20 months of age) murine lung, with marked levels of immune cells infiltrating into the aged lung (**Figure 2A**). As the course of influenza infection progressed, there was increased inflammation present in the aged lung that corresponded with increased viral titers, morbidity, and mortality (**Figure 2A-B**, **Supplemental Figure 1B-C**). Examination of the total bronchoalveolar lavage (BAL) cell count illustrated significantly increased cellular infiltration in aged lung (**Figure 2C**). Lung permeability was assessed by intranasal instillation of FITC-dextran. As shown in Figure 2D, there was a significant increase in lung permeability, as illustrated by

elevated FITC fluorescence in plasma, in aged lung at baseline as well as in response to influenza. Similarly, there was a significant increase in BAL protein that corresponded with elevated water accumulation in the aged lung during infection (Figure 2E-F). Given the importance of NAD levels in mediating tissue injury, we examined changes in NAD^+ expression in young and aged lung tissue. Our results illustrated an age-dependent decrease in NAD^+ in lung tissue at baseline and during the course of infection (Figure 2G). When compared to young, there was increased expression of IL6 and IL1β by day 5, with significantly enhanced production by day 7 (**Figure 2H-I**). Initial expression of resolution cytokines, such as IL10, was detectable in the BAL collected on day 7 post infection, with a significantly higher-level present in BAL isolated from young lung (**Figure 2J**). We next examined if heightened IL10 expression correlated with increased infiltration of $CD4^+CD25^+$ regulatory T cells. When compared to young, despite increased baseline $CD4^+CD25^+$ T cell numbers in aged lung, there were significantly decreased number of cells present in aged lung in response to influenza (**Figure 2K**).

We observed that metabolic profiles of young and aged lung samples cluster separately at baseline as well as during influenza (**Figure 3A**). Focusing on the biochemical and pathway changes in the profiles, illustrated an important role for kynurenine and tryptophan metabolism in modulating immune responses in the lung in response to influenza (**Figure 3B**). Specifically, kynurenine was increasingly elevated over time in lung isolated from both young and aged adult mice, with significantly higher levels being detected in the young lung at day 7 post infection (**Figure 3C**). While levels of kynurenate were similar in young and aged lung, the kynurenine catabolite, quinolinate, was augmented in young lung at later time points of influenza infection (**Figure 3D-E**). There was an increase in the presence of tryptophan in the aged lung, with significantly higher levels present at day 7 of influenza infection (**Figure 3F**). Increased expression of

downstream tryptophan metabolites, indoleacetate and indolepropionate, were also detected in aged lung at later time points of infection (**Figure 3G-H**).

We next examined if changes in IDO1 expression and activity in aged lung might underlie changes in tryptophan metabolism in response to influenza. In response to influenza, there was significantly reduced IDO1 specific activity at days 5 and 7 post infection in both lung and BAL collected from aged adult mice (**Figure 4A-B**). Levels of kynurenine in lung and BAL illustrated a similar phenotype in aged mice, with significantly higher levels at baseline that decline during the course of influenza infection (**Figure 4C-D**). A corresponding increase in tryptophan was also present in aged lung and BAL, with significantly increased expression at days 5 and 7 post infection (**Figure 4E-F**).

IDO1 inhibition in young macrophages and lung contribute to increased IL6 expression and inflammation during infection.

To elucidate the importance of IDO1 for influenza mediated production of inflammatory cytokines, such as IL6, we examined the impact of several IDO1 inhibitors on modulating IL6 production by young BMDM in response to LPS or poly I:C stimulation. In response to stimulation with LPS (24 hours) there was a significant increase in IL6 production by young BMDM treated with IDO1 inhibitors BMS-986205, 1-methyl-DL-tryptophan, NLG919, and IDO-1 inhibitor (**Supplemental Figure 2A**). In response to poly I:C stimulation (24 hours), there was a significant increase in IL6 production by young BMDM treated with IDO1 inhibitors BMS-986205, NLG919, and IDO-1 inhibitor (**Supplemental Figure 2B**). Based on these results, we chose to further examine the impact of IDO1 inhibition using the irreversible inhibitor, BMS-986205. Treatment of

young BMDM with BMS-986205 resulted in a significant decrease in IDO1 protein expression and activity, which corresponded with increased IL6 production (**Supplemental Figure 2C-E**). Daily *in vivo* treatment of young adult mice with BMS-986205 resulted in increased cellular infiltration and marked changes in the lung that corresponded with significant weight loss and increased viral titers (**Figure 5A-D**). In response to BMS-986205, there was a significant increase in cells present in the BAL that corresponded with decreased IDO1 activity in lung and alveolar macrophage populations and significantly augmented levels of pro-inflammatory cytokines, such as IL6, and decreased production of pro-resolution cytokines, such as IL10 (**Figure 5E-I**).

Age-associated mitochondrial dysfunction contributes to changes in IDO1 expression and KP mediated metabolism of tryptophan.

As shown in **Figure 6A**, when compared to young, there was reduced Ido1 mRNA expression in aged lung at baseline and during the course of influenza infection. Interestingly, there was augmented expression of other metabolic pathways, such as betaine-homocysteine methyltransferase (Bhmt), which catalyzes the conversion of homocysteine to methionine, and succinyl-CoA:3-ketoacid coenzyme A transferase 2A (Oxct2a), a key enzyme for ketone body catabolism, in aged lung by day 7 post influenza (**Figure 6A, Supplemental Table 1**). When compared to young, there was also diminished Ido1 mRNA expression in aged alveolar macrophages during the course of influenza infection (**Figure 6B, Supplemental Table 1).** Decreased kynurenine 3-monooxygenase (Kmo) and nitric oxide synthase 2 (Nos2) mRNA expression, which was associated with augmented Oxct2a mRNA expression, was observed in aged alveolar macrophages by day 7 of influenza infection (**Figure 6B, Supplemental Table 1**). As mitochondria play an intricate role in modulating metabolic processes, we next examined

how different components of the mitochondria might respond to energy demands of the host during influenza infection. During influenza infection, there were distinct changes in gene regulation in both young and aged lung, with decreased gene expression in aged lung by day 7 of infection (**Figure 6C and Supplemental Table 2**). Recent work has illustrated that kynurenine can bind to aryl hydrocarbon receptor and result in heightened kynurenine activity [21]. Interestingly, in aged lung by day 7 of influenza, there was upregulated expression of AhR interacting protein (Aip), a protein shown to stabilize and enhance AhR function, which corresponded with declining levels of kynurenine [22] (**Figure 6C, Supplemental Table 2**).

Given these findings, we evaluated the impact of mitochondrial targeted antioxidants, mitoTEMPO-L (MTL), Trolox, and mitoquinol, on IL6 production by LPS stimulated BMDM. There was a significant reduction of IL6 at both 4 and 24 hours in aged, mitoquinol treated BMDM (**Supplemental Figure 3A**). Further, in response to treatment of aged BMDM with mitoquinol, there was a significant increase in IDO1 expression, increased ratio of kynurenine to tryptophan post stimulation with LPS and poly I:C, and a corresponding decrease in IL6 production (**Supplemental Figure 3B-D**). Based on these findings, we treated aged mice with daily injections of mitoquinol (50μM/mouse/day) starting at a time point when clinical manifestations of influenza were detectable in aged mice (day 3 post infection) (**Supplemental Figure 4A**). In response to mitoquinol, there was a marked decrease in weight loss and decreased viral titers (**Supplemental Figure 4B-C**). Further, mitoquinol treatment dramatically impacted mitochondrial gene expression in aged lung on day 7 post influenza (**Figure 6C, Supplemental Table 3**). Specifically, mitoquinol treatment resulted in decreased expression of Aip (**Figure 6C, Supplemental Table 3).** Superoxide formation in alveolar macrophages isolated from lung at select time points during influenza was also

decreased in response to mitoquinol treatment (**Supplemental Figure 4D**). In response to daily treatment with mitoquinol there was a significant decrease in Bhmt and Oxct2a mRNA that was associated with increased IDO1 mRNA expression in aged lung by day 7 post influenza (**Figure 6D, Supplemental Table 2**). Examination of metabolic gene expression in aged alveolar macrophages at days 5 and 7 post influenza infection, illustrated a decrease in Oxct2a mRNA and a corresponding increase in Ido1 and Kmo mRNA expression (**Figure 6E**, **Supplemental Table 2**).

In response to different doses of mitoquinol, we detected increased IDO1 specific activity, which corresponded with significantly heightened kynurenine and reduced tryptophan production (**Figure 7A-C**). Daily treatment with mitoquinol decreased cellular infiltration and inflammation in the aged lung (**Figure 7D-E**). Further, at day 7 post influenza, there was a significant reduction of IL6 expression in BAL and lung homogenates collected from mitoquinol treated mice (**Figure 7F**). Further, in response to daily treatment with mitoquinol, there was a dose dependent increase in the number of $CD4^{+}CD25^{+}$ T regulatory cells, which corresponded with increasing levels of IL10 production in aged lung by day 7 post influenza (**Figure 7G-H**).

Discussion

In the current study, we investigated the impact of chronological aging on tryptophan metabolism in response to influenza infection. Examination of metabolites present in human plasma, identified tryptophan metabolism as an important metabolic pathway utilized in response to influenza. Our results expand upon these findings and illustrate decreased production of kynurenine in aged lung in response to influenza was associated with increased inflammatory and diminished regulatory responses. Reduced

IDO1 activity in aged lung and alveolar macrophages corresponded with changes in metabolic gene regulation and the initiation of alternative tryptophan metabolism pathways. Our findings also demonstrated that decreased IDO1 expression was due to dysregulated mitochondrial gene expression and heightened generation of ROS, as treatment with mitoquinol improved mitochondrial function and restored KP mediated tryptophan metabolism. Taken together, our data provide additional evidence as to why older persons are more susceptible to influenza.

Using a murine model of infection, there was an increase in kynurenine in both young and aged lung starting at day 3 and continued to increase by day 5. These findings are in agreement with previous influenza studies investigating the metabolic responses in young adult mice [23]. However, by day 7, kynurenine levels were only heightened in young lung, with levels remaining unchanged in the aged lung. While kynurenine was produced by an inflammatory process, it has an anti-inflammatory function, often serving as a brake on the immune response. Downstream metabolites, such as quinolinate, play an important role in replenishing NAD^+ levels to meet host energy demands in response to heightened cellular stress during influenza infection. Decreased KP mediated tryptophan metabolism and production of quinolinate in aged lung corresponded with impaired NAD^+ replenishment and an inability to meet host energy demands. As tryptophan metabolism is a negative feedback metabolism, an inefficacy of aged alveolar macrophages to utilize this metabolic pathway would result in decreased NAD^+ replenishment and increased inflammation. Interestingly, kynurenine levels appeared to be higher in the older animals at baseline but increased more dramatically in the young animals following infection. Previous work has illustrated that chronic low-grade inflammation can result in elevated levels of circulating kynurenine [24]. Therefore, it may be possible that the increased presence of inflammatory cytokines in aged hosts

may have a significant impact on baseline kynurenine levels and resulting in changes in tryptophan metabolism in response to pathogenic stimuli.

During the course of influenza infection, there was a metabolic shift in aged lung and alveolar macrophages. When compared to young, there was an increase in succinyl-coA: 3-ketoacid coenzyme A transferase 2A (Oxct2a), a key enzyme for ketone body catabolism, which corresponded with diminished mitochondrial gene expression. Our results illustrate that treatment with a mitochondrial targeted antioxidant improved mitochondrial gene regulation and diminished Oxct2a expression in aged lung and alveolar macrophages. Based on these findings, during the course of influenza, when there is decreased glycolytic ATP production, to meet host energy demands, there may be a change in metabolic gene expression, which may reflect increased ketone body catabolism. In the context of heightened cellular stress and energy deficiency that occurs in response to influenza, macrophage utilization of ketone bodies may help to regulate TCA cycle flux, modulate pyruvate-derived gluconeogenesis, and serve as an alternative source of ATP [25]. Metabolic reprogramming of macrophages in response to influenza highlights an age associated impact on the phenotypic characteristics that may impact not only the antimicrobial properties, but also influence dysregulated tissue repair and remodelling.

Our current results illustrate that daily administration of mitoquinol to aged adult mice improves IDO1 mediated metabolism of tryptophan to kynurenine; thereby, improving host innate immune responses and decreasing morbidity and mortality during the course of influenza. It is well appreciated that ROS signalling plays a key role in the initiation of innate immune responses during influenza, however overly heightened ROS production can result in excessive immune responses and have a deleterious impact on host tissue

systems. Designed as a lipophilic molecule bearing a cation moiety, mitoquinol can pass directly through the mitochondrial membrane to increase the mitochondrial antioxidant capacity and decrease mitochondrial oxidative damage [26]. Further, mitoquinol can function as an antioxidant to prevent lipid peroxidation-induced apoptosis and protect mitochondria from oxidative damage [27]. Mitoquinol has been previously shown to be efficacious in reducing mitochondrial oxidative damage in multiple diseases, such as sepsis, fatty liver disease, and Alzheimer's disease [27, 28]. Future work will need to be performed to understand the exact mechanistic pathways that are altered in response to mitoquinol treatment and if therapeutic administration of mitoquinol in additional pulmonary viral infection models will also prove to be efficacious.

It is important to note that IDO1 expression by epithelial cells and fibroblasts can also influence regulatory responses at the site of inflammation [29, 30]. Recent work has illustrated that expression of IDO in lung parenchyma can inhibit acute lethal pulmonary inflammation [31]. Specifically, the production of kynurenine by lung epithelial cells as well as alveolar macrophages can suppress inflammatory activities within the lung [31]. In agreement with these findings, when young adult mice were treated with IDO1 inhibitor, BMS-986205, there was a significant increase in inflammation and heightened lung injury during influenza infection. It is plausible, that in the absence of IDO1 activity and diminished kynurenine production, there is an inability of epithelial and alveolar macrophages to inhibit inflammation, resulting in increased morbidity and mortality during influenza. Previous work has illustrated that IDO1-deficient and 1-methyltryptophan treated mice are protected from morbidity during influenza A infection [4]. It is important to note that these studies examined the impact of IDO1 deficiency in young mice and it is possible that compensatory pathways may contribute to protection during influenza. Our data in young adult mice using BMS-986205 also illustrated an

increase in morbidity during infection. We believe that this is due to the potent and selective IDO1 inhibitory properties of this compound when compared to 1-methyltryptophan, which has been shown to not induce effective in vivo IDO inhibition due to decreased potency and similar plasma concentrations of tryptophan post treatment [32]. While our current work focused on alveolar macrophages, future studies will need to investigate the contribution of epithelial cell production of kynurenine during influenza and the impact of aging on these responses.

References

1. Iuliano AD, Roguski KM, Chang HH, Muscatello DJ, Palekar R, Tempia S, Cohen C, Gran JM, Schanzer D, Cowling BJ, Wu P, Kyncl J, Ang LW, Park M, Redlberger-Fritz M, Yu H, Espenhain L, Krishnan A, Emukule G, van Asten L, Pereira da Silva S, Aungkulanon S, Buchholz U, Widdowson MA, Bresee JS, Global Seasonal Influenza-associated Mortality Collaborator N. Estimates of global seasonal influenza-associated respiratory mortality: a modelling study. *Lancet* 2018: 391(10127): 1285-1300.

2. Gaelings L, Soderholm S, Bugai A, Fu Y, Nandania J, Schepens B, Lorey MB, Tynell J, Vande Ginste L, Le Goffic R, Miller MS, Kuisma M, Marjomaki V, De Brabander J, Matikainen S, Nyman TA, Bamford DH, Saelens X, Julkunen I, Paavilainen H, Hukkanen V, Velagapudi V, Kainov DE. Regulation of kynurenine biosynthesis during influenza virus infection. *FEBS J* 2017: 284(2): 222-236.

3. Fox JM, Sage LK, Huang L, Barber J, Klonowski KD, Mellor AL, Tompkins SM, Tripp RA. Inhibition of indoleamine 2,3-dioxygenase enhances the T-cell response to influenza virus infection. *J Gen Virol* 2013: 94(Pt 7): 1451-1461.

4. Huang L, Li L, Klonowski KD, Tompkins SM, Tripp RA, Mellor AL. Induction and role of indoleamine 2,3 dioxygenase in mouse models of influenza a virus infection. *PLoS One* 2013: 8(6): e66546.

5. Taylor MW, Feng GS. Relationship between interferon-gamma, indoleamine 2,3-dioxygenase, and tryptophan catabolism. *FASEB J* 1991: 5(11): 2516-2522.

6. Frumento G, Rotondo R, Tonetti M, Damonte G, Benatti U, Ferrara GB. Tryptophan-derived catabolites are responsible for inhibition of T and natural killer cell proliferation induced by indoleamine 2,3-dioxygenase. *J Exp Med* 2002: 196(4): 459-468.

7. Fallarino F, Grohmann U, Vacca C, Bianchi R, Orabona C, Spreca A, Fioretti MC, Puccetti P. T cell apoptosis by tryptophan catabolism. *Cell Death Differ* 2002: 9(10): 1069-1077.

8. Belladonna ML, Puccetti P, Orabona C, Fallarino F, Vacca C, Volpi C, Gizzi S, Pallotta MT, Fioretti MC, Grohmann U. Immunosuppression via tryptophan catabolism: the role of kynurenine pathway enzymes. *Transplantation* 2007: 84(1 Suppl): S17-20.

9. Mezrich JD, Fechner JH, Zhang X, Johnson BP, Burlingham WJ, Bradfield CA. An interaction between kynurenine and the aryl hydrocarbon receptor can generate regulatory T cells. *J Immunol* 2010: 185(6): 3190-3198.

10. Grant RS, Passey R, Matanovic G, Smythe G, Kapoor V. Evidence for increased de novo synthesis of NAD in immune-activated RAW264.7 macrophages: a self-protective mechanism? *Arch Biochem Biophys* 1999: 372(1): 1-7.

11. Chen W, Liang X, Peterson AJ, Munn DH, Blazar BR. The indoleamine 2,3-dioxygenase pathway is essential for human plasmacytoid dendritic cell-induced adaptive T regulatory cell generation. *J Immunol* 2008: 181(8): 5396-5404.

12. Jurgens B, Hainz U, Fuchs D, Felzmann T, Heitger A. Interferon-gamma-triggered indoleamine 2,3-dioxygenase competence in human monocyte-derived dendritic cells induces regulatory activity in allogeneic T cells. *Blood* 2009: 114(15): 3235-3243.

13. Robinson CM, Hale PT, Carlin JM. The role of IFN-gamma and TNF-alpha-responsive regulatory elements in the synergistic induction of indoleamine dioxygenase. *J Interferon Cytokine Res* 2005: 25(1): 20-30.

14. Hassanain HH, Chon SY, Gupta SL. Differential regulation of human indoleamine 2,3-dioxygenase gene expression by interferons-gamma and -alpha. Analysis of the regulatory region of the gene and identification of an interferon-gamma-inducible DNA-binding factor. *J Biol Chem* 1993: 268(7): 5077-5084.

15. Chaves AC, Ceravolo IP, Gomes JA, Zani CL, Romanha AJ, Gazzinelli RT. IL-4 and IL-13 regulate the induction of indoleamine 2,3-dioxygenase activity and the control of Toxoplasma gondii replication in human fibroblasts activated with IFN-gamma. *Eur J Immunol* 2001: 31(2): 333-344.

16. Ma KC, Schenck EJ, Siempos, II, Cloonan SM, Finkelsztein EJ, Pabon MA, Oromendia C, Ballman KV, Baron RM, Fredenburgh LE, Higuera A, Lee JY, Chung CR, Jeon K, Yang JH, Howrylak JA, Huh JW, Suh GY, Choi AM. Circulating RIPK3 levels are associated with mortality and organ failure during critical illness. *JCI Insight* 2018: 3(13).

17. Finkelsztein EJ, Jones DS, Ma KC, Pabon MA, Delgado T, Nakahira K, Arbo JE, Berlin DA, Schenck EJ, Choi AM, Siempos, II. Comparison of qSOFA and SIRS for predicting adverse outcomes of patients with suspicion of sepsis outside the intensive care unit. *Crit Care* 2017: 21(1): 73.

18. Dolinay T, Kim YS, Howrylak J, Hunninghake GM, An CH, Fredenburgh L, Massaro AF, Rogers A, Gazourian L, Nakahira K, Haspel JA, Landazury R, Eppanapally S, Christie JD, Meyer NJ, Ware LB, Christiani DC, Ryter SW, Baron RM, Choi AM. Inflammasome-regulated cytokines are critical mediators of acute lung injury. *Am J Respir Crit Care Med* 2012: 185(11): 1225-1234.

19. Park J, Pabon M, Choi AMK, Siempos, II, Fredenburgh LE, Baron RM, Jeon K, Chung CR, Yang JH, Park CM, Suh GY. Plasma surfactant protein-D as a diagnostic biomarker for acute respiratory distress syndrome: validation in US and Korean cohorts. *BMC Pulm Med* 2017: 17(1): 204.

20. Schenck EJ, Ma KC, Price DR, Nicholson T, Oromendia C, Gentzler ER, Sanchez E, Baron RM, Fredenburgh LE, Huh JW, Siempos, II, Choi AM. Circulating cell death biomarker TRAIL is associated with increased organ dysfunction in sepsis. *JCI Insight* 2019: 4(9).

21. Seok SH, Ma ZX, Feltenberger JB, Chen H, Chen H, Scarlett C, Lin Z, Satyshur KA, Cortopassi M, Jefcoate CR, Ge Y, Tang W, Bradfield CA, Xing Y. Trace derivatives of kynurenine potently activate the aryl hydrocarbon receptor (AHR). *J Biol Chem* 2018: 293(6): 1994-2005.

22. Bell DR, Poland A. Binding of aryl hydrocarbon receptor (AhR) to AhR-interacting protein. The role of hsp90. *J Biol Chem* 2000: 275(46): 36407-36414.

23. Chandler JD, Hu X, Ko EJ, Park S, Lee YT, Orr M, Fernandes J, Uppal K, Kang SM, Jones DP, Go YM. Metabolic pathways of lung inflammation revealed by high-resolution metabolomics (HRM) of H1N1 influenza virus infection in mice. *Am J Physiol Regul Integr Comp Physiol* 2016: 311(5): R906-R916.

24. Dantzer R. Role of the Kynurenine Metabolism Pathway in Inflammation-Induced Depression: Preclinical Approaches. *Curr Top Behav Neurosci* 2017: 31: 117-138.

25. Newman JC, Verdin E. Ketone bodies as signaling metabolites. *Trends Endocrinol Metab* 2014: 25(1): 42-52.

26. Kelso GF, Porteous CM, Coulter CV, Hughes G, Porteous WK, Ledgerwood EC, Smith RA, Murphy MP. Selective targeting of a redox-active ubiquinone to mitochondria within cells: antioxidant and antiapoptotic properties. *J Biol Chem* 2001: 276(7): 4588-4596.

27. Gane EJ, Weilert F, Orr DW, Keogh GF, Gibson M, Lockhart MM, Frampton CM, Taylor KM, Smith RA, Murphy MP. The mitochondria-targeted anti-oxidant mitoquinone decreases liver damage in a phase II study of hepatitis C patients. *Liver Int* 2010: 30(7): 1019-1026.

28. Smith RA, Hartley RC, Murphy MP. Mitochondria-targeted small molecule therapeutics and probes. *Antioxid Redox Signal* 2011: 15(12): 3021-3038.

29. Aldajani WA, Salazar F, Sewell HF, Knox A, Ghaemmaghami AM. Expression and regulation of immune-modulatory enzyme indoleamine 2,3-dioxygenase (IDO) by

human airway epithelial cells and its effect on T cell activation. *Oncotarget* 2016: 7(36): 57606-57617.

30. Curran TA, Jalili RB, Farrokhi A, Ghahary A. IDO expressing fibroblasts promote the expansion of antigen specific regulatory T cells. *Immunobiology* 2014: 219(1): 17-24.

31. Lee SM, Park HY, Suh YS, Yoon EH, Kim J, Jang WH, Lee WS, Park SG, Choi IW, Choi I, Kang SW, Yun H, Teshima T, Kwon B, Seo SK. Inhibition of acute lethal pulmonary inflammation by the IDO-AhR pathway. *Proc Natl Acad Sci U S A* 2017: 114(29): E5881-E5890.

32. Gunther J, Dabritz J, Wirthgen E. Limitations and Off-Target Effects of Tryptophan-Related IDO Inhibitors in Cancer Treatment. *Front Immunol* 2019: 10: 1801.

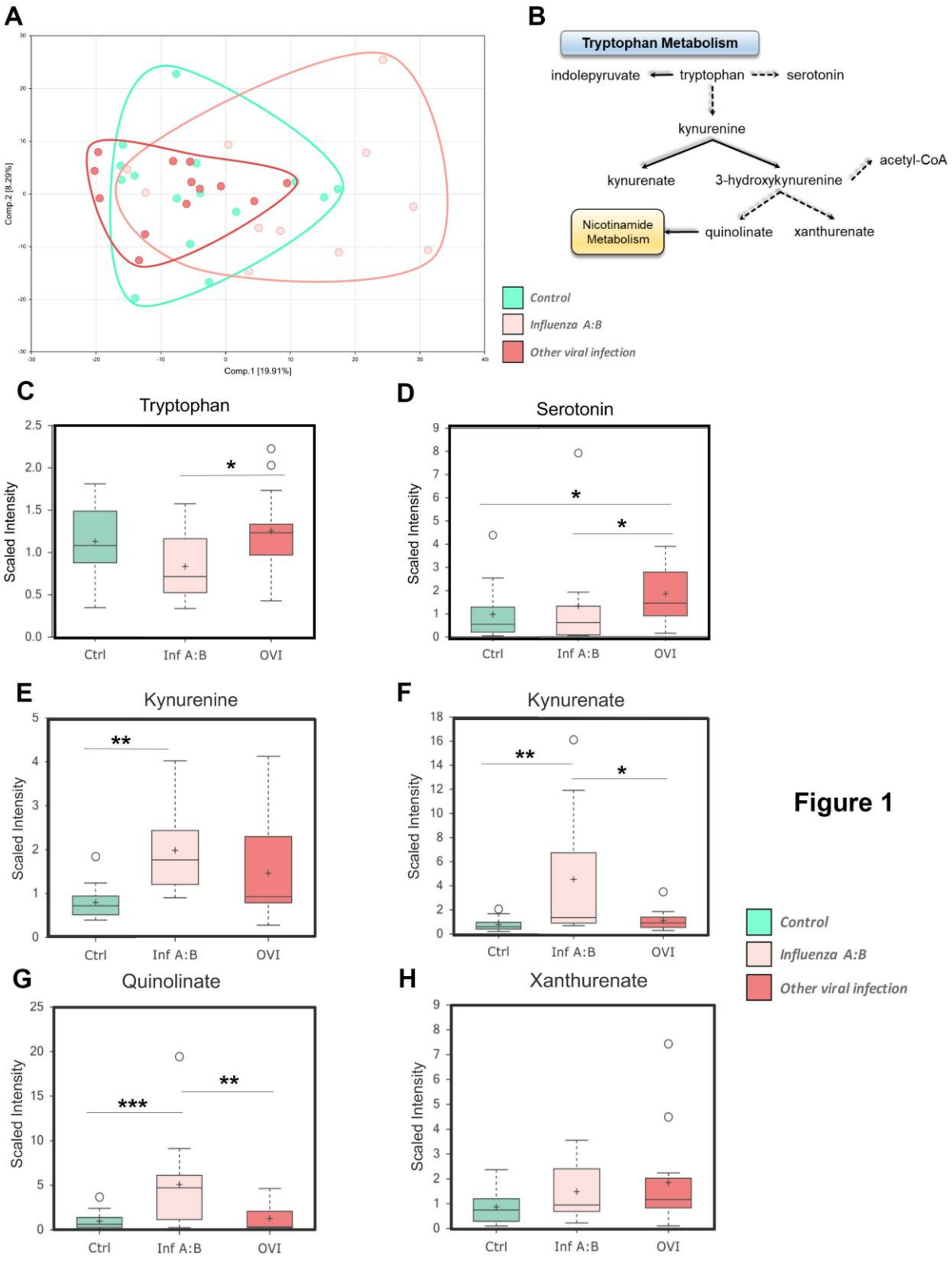
A
Comp.1 [19.91%]
Comp.2 [8.29%]
B
Tryptophan Metabolism
indolepyruvate
tryptophan
serotonin
kynurenine
kynurenate
3-hydroxykynurenine
acetyl-CoA
Nicotinamide Metabolism
quinolinate
xanthurenate
Control
Influenza A:B
Other viral infection
C
Tryptophan
D
Serotonin
E
Kynurenine
F
Kynurenate
G
Quinolinate
H
Xanthurenate
Scaled Intensity
Ctrl
Inf A:B
OVI

Figure 1

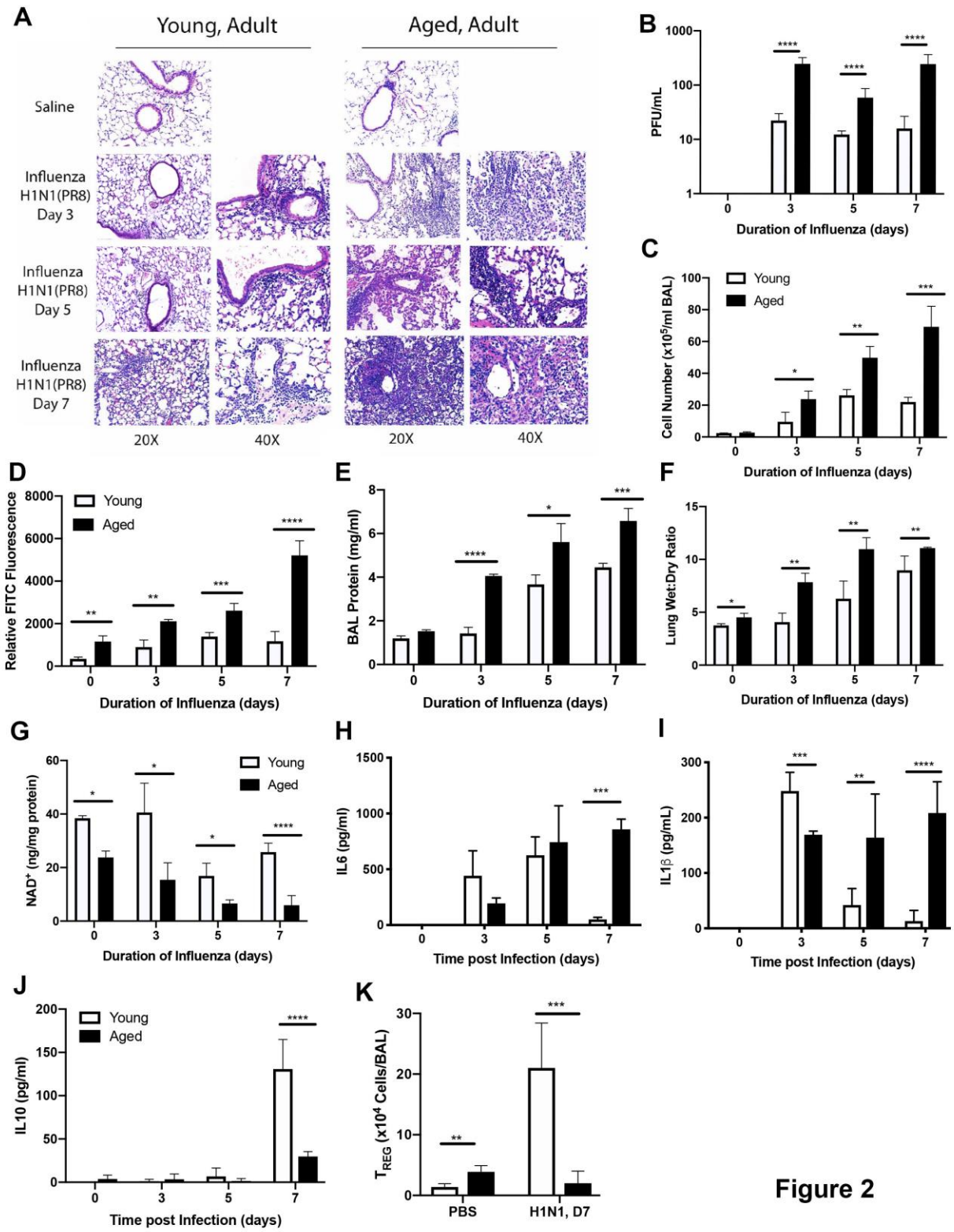
A
Young, Adult
Aged, Adult
Saline
Influenza H1N1(PR8) Day 3
Influenza H1N1(PR8) Day 5
Influenza H1N1(PR8) Day 7
20X
40X
20X
40X
B
PFU/mL
Duration of Influenza (days)
C
Young
Aged
Cell Number (x10^5/ml BAL)
Duration of Influenza (days)
D
Young
Aged
Relative FITC Fluorescence
Duration of Influenza (days)
E
BAL Protein (mg/ml)
Duration of Influenza (days)
F
Lung Wet:Dry Ratio
Duration of Influenza (days)
G
Young
Aged
NAD+ (ng/mg protein)
Duration of Influenza (days)
H
IL6 (pg/ml)
Time post Infection (days)
I
IL1β (pg/mL)
Time post Infection (days)
J
Young
Aged
IL10 (pg/ml)
Time post Infection (days)
K
T_REG (x10^4 Cells/BAL)
PBS
H1N1, D7

Figure 2

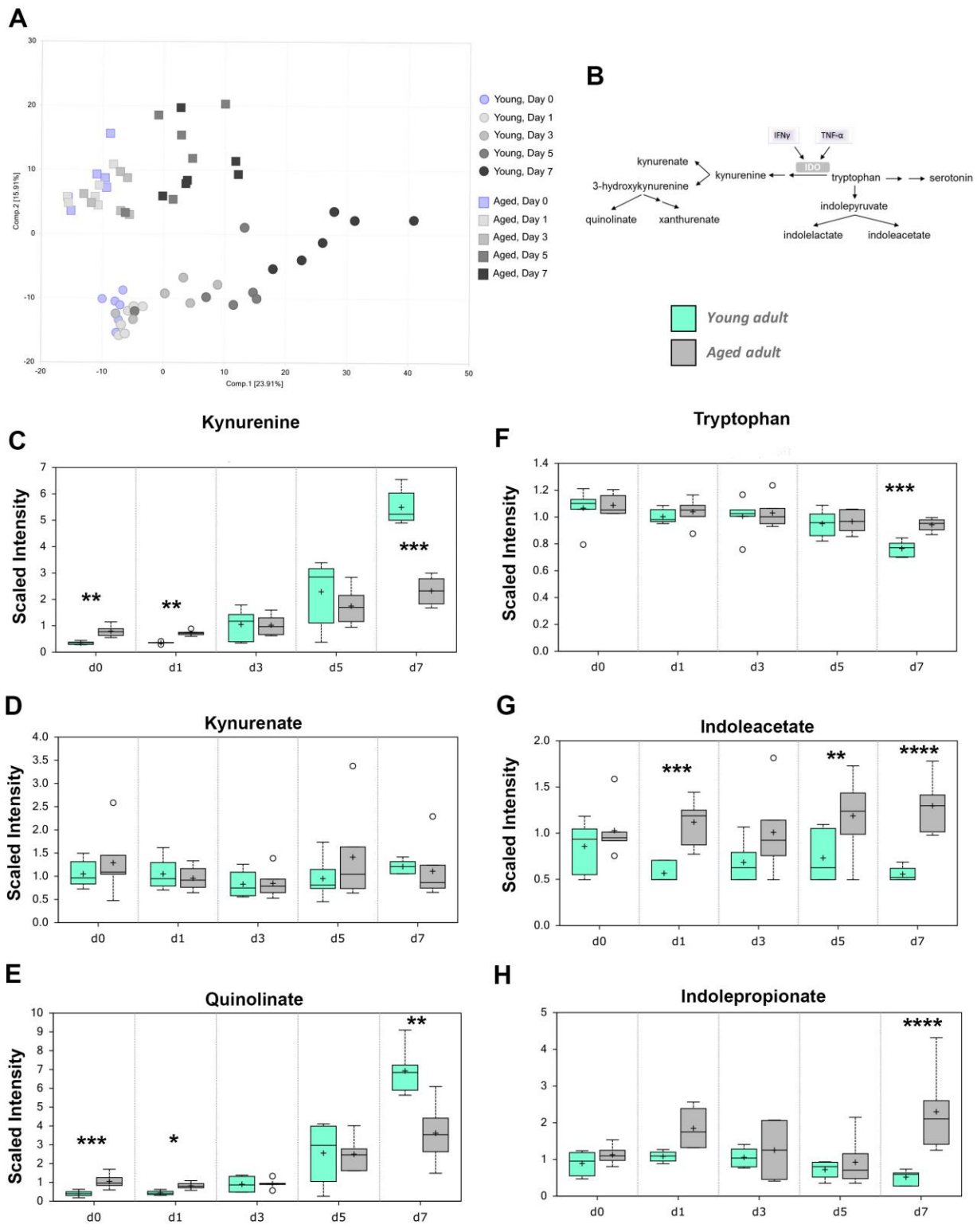
A
Young, Day 0
Young, Day 1
Young, Day 3
Young, Day 5
Young, Day 7
Aged, Day 0
Aged, Day 1
Aged, Day 3
Aged, Day 5
Aged, Day 7
Comp.1 [23.91%]
Comp.2 [15.91%]
B
IFNγ
TNF-α
IDO
kynurenate
kynurenine
3-hydroxykynurenine
quinolinate
xanthurenate
tryptophan
serotonin
indolepyruvate
indolelactate
indoleacetate
Young adult
Aged adult
C
Kynurenine
Scaled Intensity
d0
d1
d3
d5
d7
F
Tryptophan
D
Kynurenate
G
Indoleacetate
E
Quinolinate
H
Indolepropionate

Figure 3

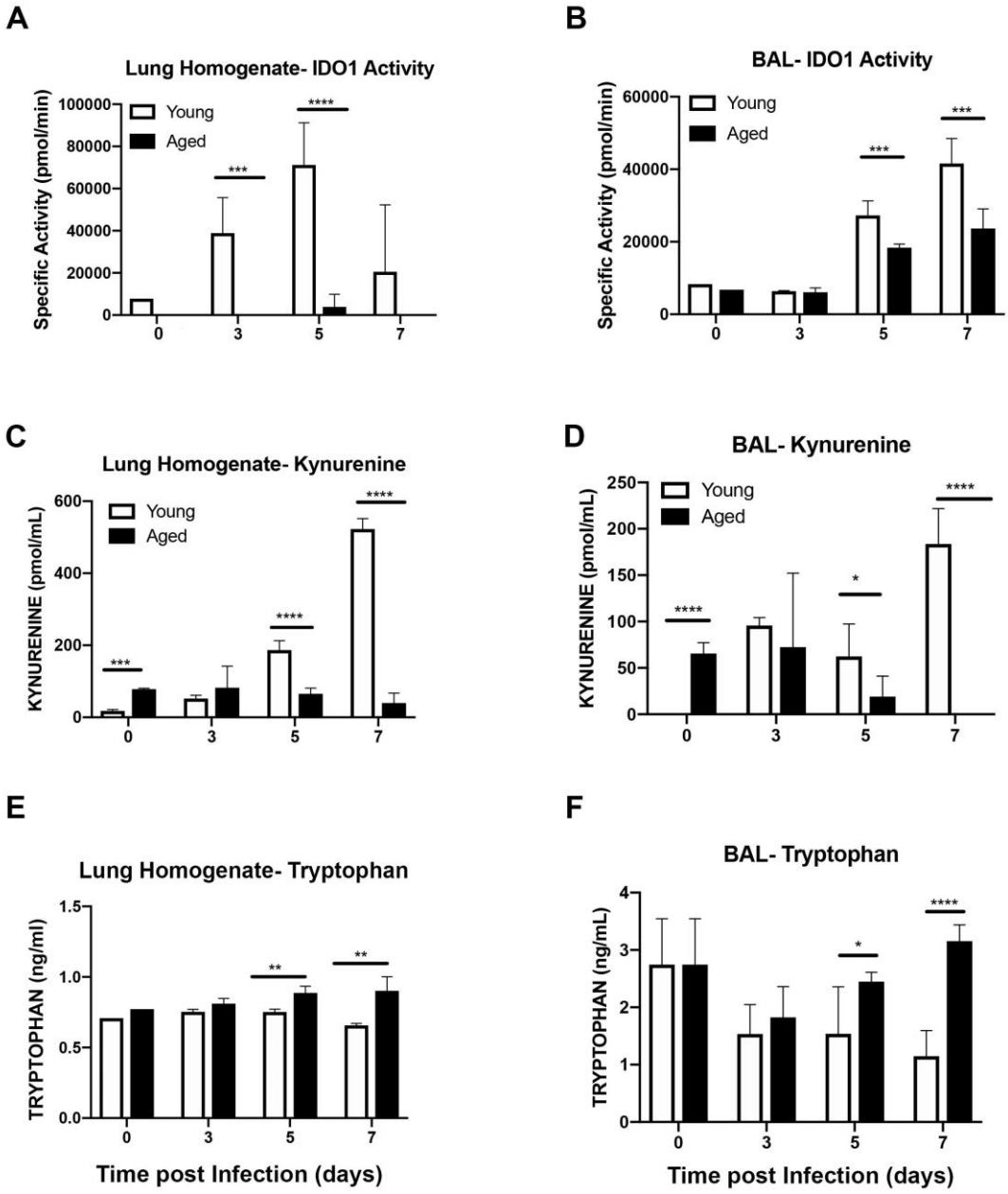
A
Lung Homogenate- IDO1 Activity
Specific Activity (pmol/min)
Young
Aged
B
BAL- IDO1 Activity
Specific Activity (pmol/min)
C
Lung Homogenate- Kynurenine
KYNURENINE (pmol/mL)
D
BAL- Kynurenine
KYNURENINE (pmol/mL)
E
Lung Homogenate- Tryptophan
TRYPTOPHAN (ng/ml)
F
BAL- Tryptophan
TRYPTOPHAN (ng/mL)
Time post Infection (days)

Figure 4

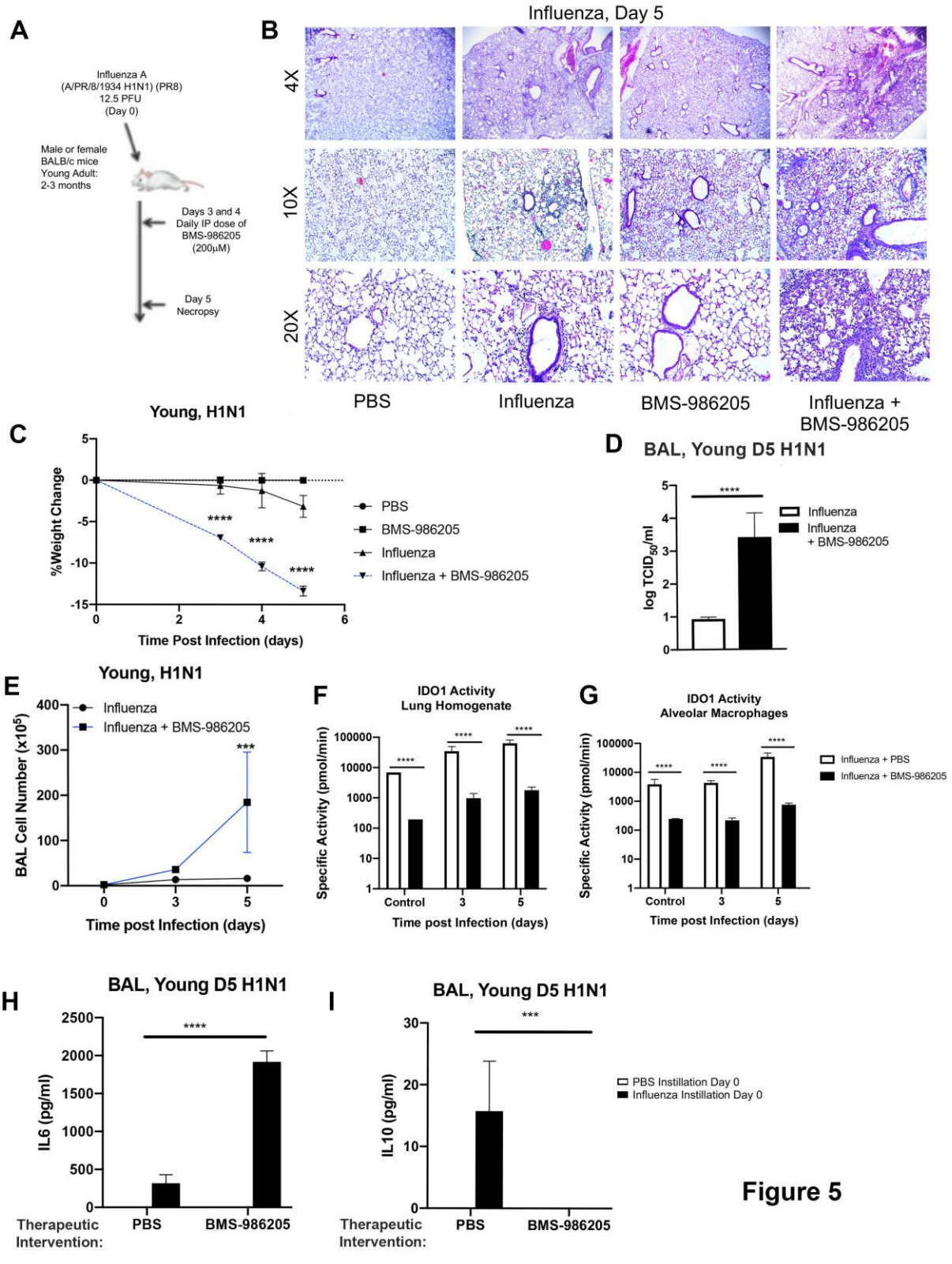
A
Influenza A
(A/PR/8/1934 H1N1) (PR8)
12.5 PFU
(Day 0)
Male or female
BALB/c mice
Young Adult:
2-3 months
Days 3 and 4
Daily IP dose of
BMS-986205
(200μM)
Day 5
Necropsy
B
Influenza, Day 5
4X
10X
20X
PBS
Influenza
BMS-986205
Influenza +
BMS-986205
C
Young, H1N1
%Weight Change
Time Post Infection (days)
PBS
BMS-986205
Influenza
Influenza + BMS-986205
D
BAL, Young D5 H1N1
log TCID50/ml
Influenza
Influenza
+ BMS-986205
E
Young, H1N1
BAL Cell Number (x10^5)
Influenza
Influenza + BMS-986205
Time post Infection (days)
F
IDO1 Activity
Lung Homogenate
Specific Activity (pmol/min)
Control
Time post Infection (days)
G
IDO1 Activity
Alveolar Macrophages
Specific Activity (pmol/min)
Influenza + PBS
Influenza + BMS-986205
Time post Infection (days)
H
BAL, Young D5 H1N1
IL6 (pg/ml)
Therapeutic
Intervention:
PBS
BMS-986205
I
BAL, Young D5 H1N1
IL10 (pg/ml)
PBS Instillation Day 0
Influenza Instillation Day 0
Therapeutic
Intervention:
PBS
BMS-986205

Figure 5

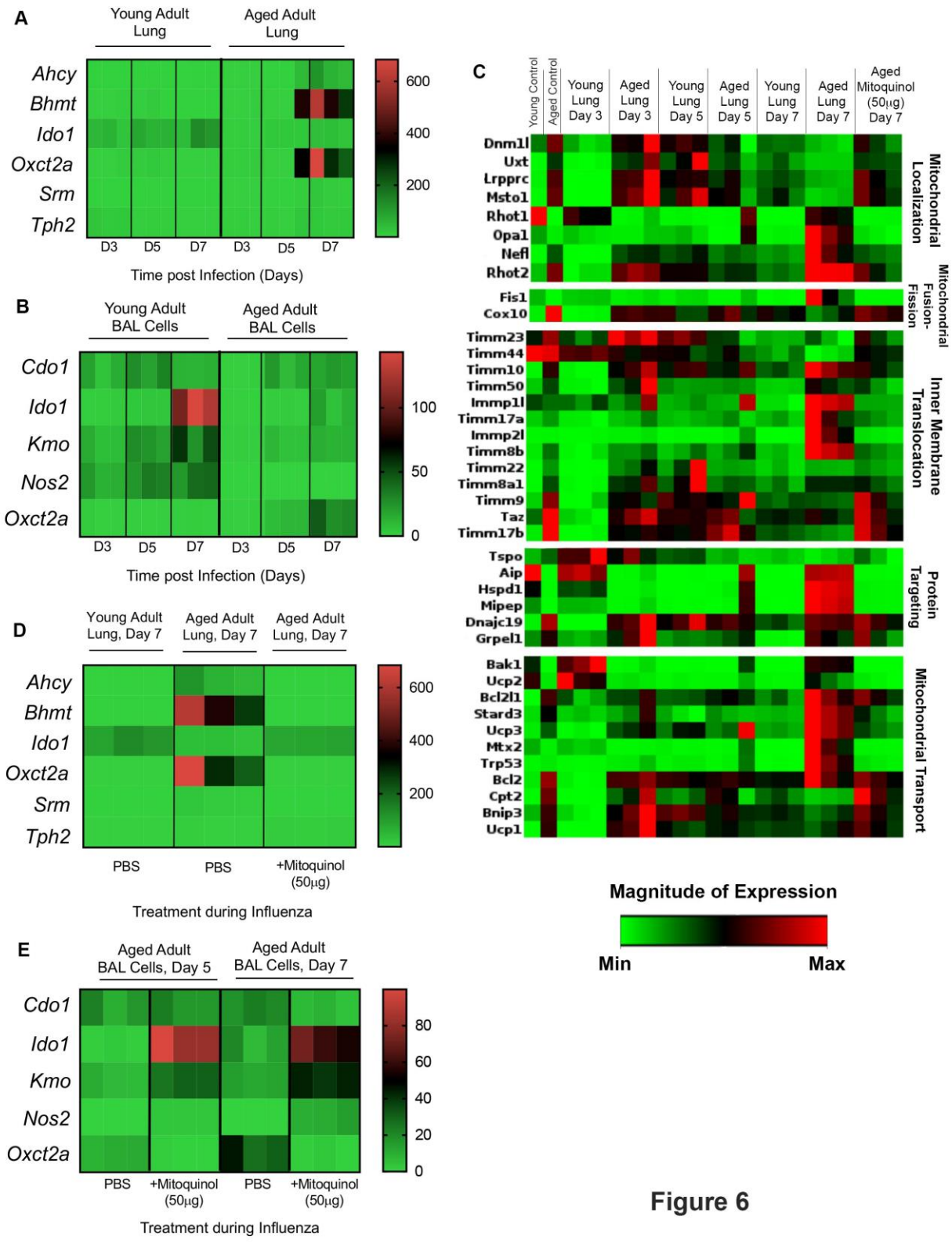
A
Young Adult Lung
Aged Adult Lung
Ahcy
Bhmt
Ido1
Oxct2a
Srm
Tph2
D3 D5 D7 D3 D5 D7
600
400
200
Time post Infection (Days)
B
Young Adult BAL Cells
Aged Adult BAL Cells
Cdo1
Ido1
Kmo
Nos2
Oxct2a
D3 D5 D7 D3 D5 D7
100
50
0
Time post Infection (Days)
D
Young Adult Lung, Day 7
Aged Adult Lung, Day 7
Aged Adult Lung, Day 7
Ahcy
Bhmt
Ido1
Oxct2a
Srm
Tph2
600
400
200
PBS
PBS
+Mitoquinol (50μg)
Treatment during Influenza
E
Aged Adult BAL Cells, Day 5
Aged Adult BAL Cells, Day 7
Cdo1
Ido1
Kmo
Nos2
Oxct2a
80
60
40
20
0
PBS
+Mitoquinol (50μg)
PBS
+Mitoquinol (50μg)
Treatment during Influenza
C
Young Control
Aged Control
Young Lung Day 3
Aged Lung Day 3
Young Lung Day 5
Aged Lung Day 5
Young Lung Day 7
Aged Lung Day 7
Aged Mitoquinol (50μg) Day 7
Dnm1l
Uxt
Lrpprc
Msto1
Rhot1
Opa1
Nefl
Rhot2
Mitochondrial Localization
Fis1
Cox10
Mitochondrial Fusion-Fission
Timm23
Timm44
Timm10
Timm50
Immp1l
Timm17a
Immp2l
Timm8b
Timm22
Timm8a1
Timm9
Taz
Timm17b
Inner Membrane Translocation
Tspo
Aip
Hspd1
Mipep
Dnajc19
Grpel1
Protein Targeting
Bak1
Ucp2
Bcl2l1
Stard3
Ucp3
Mtx2
Trp53
Bcl2
Cpt2
Bnip3
Ucp1
Mitochondrial Transport
Magnitude of Expression
Min
Max

Figure 6

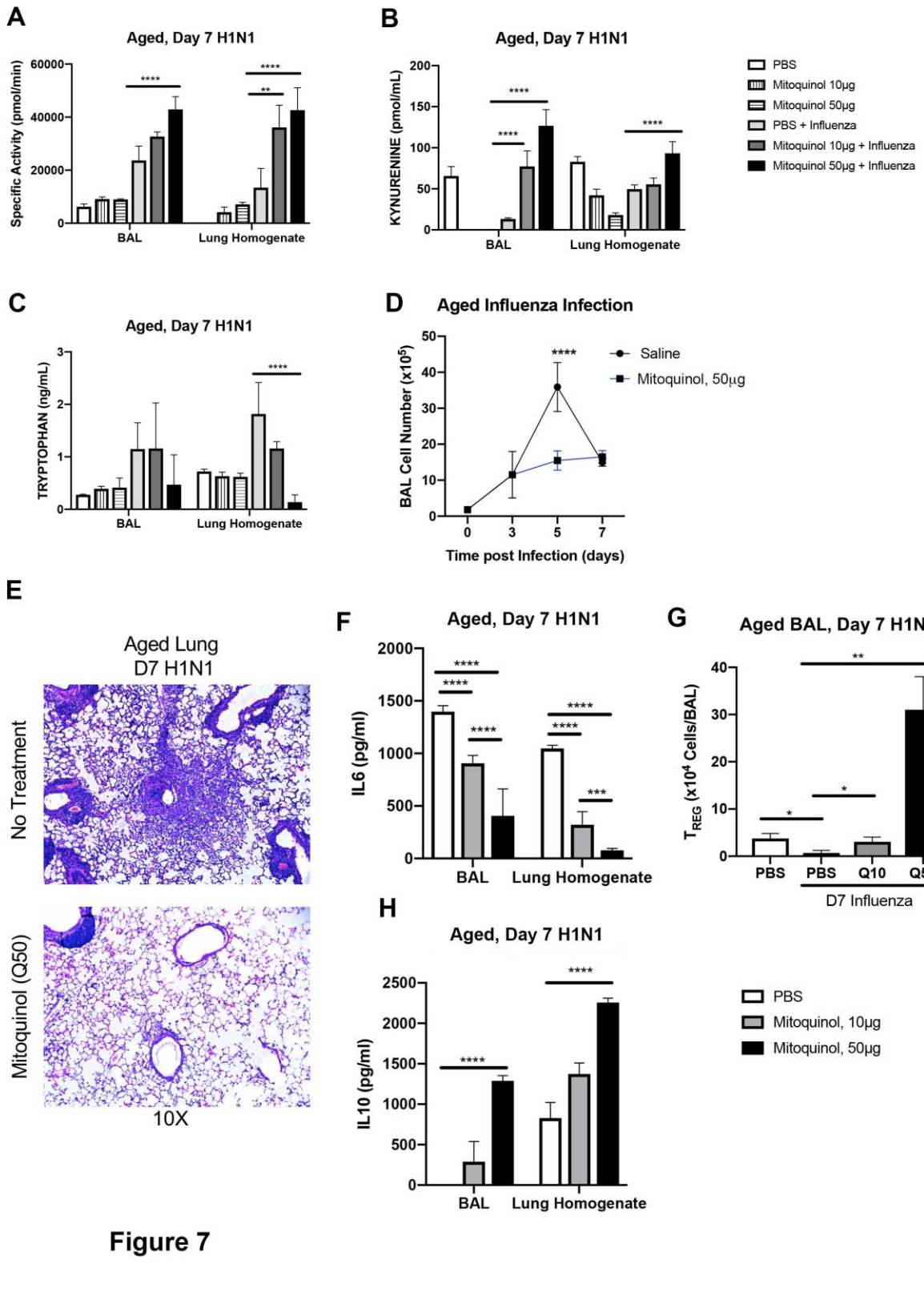
A
Aged, Day 7 H1N1
Specific Activity (pmol/min)
60000
40000
20000
0
****
****
**
BAL
Lung Homogenate
B
Aged, Day 7 H1N1
KYNURENINE (pmol/mL)
200
150
100
50
0
****
****
****
BAL
Lung Homogenate
PBS
Mitoquinol 10µg
Mitoquinol 50µg
PBS + Influenza
Mitoquinol 10µg + Influenza
Mitoquinol 50µg + Influenza
C
Aged, Day 7 H1N1
TRYPTOPHAN (ng/mL)
3
2
1
0
****
BAL
Lung Homogenate
D
Aged Influenza Infection
BAL Cell Number (x10^5)
50
40
30
20
10
0
****
Saline
Mitoquinol, 50µg
0
3
5
7
Time post Infection (days)
E
Aged Lung
D7 H1N1
No Treatment
Mitoquinol (Q50)
10X
F
Aged, Day 7 H1N1
IL6 (pg/ml)
2000
1500
1000
500
0
****
****
****
****
****
***
BAL
Lung Homogenate
G
Aged BAL, Day 7 H1N1
T_REG (x10^4 Cells/BAL)
40
30
20
10
0
**
*
*
PBS
PBS
Q10
Q50
D7 Influenza
H
Aged, Day 7 H1N1
IL10 (pg/ml)
2500
2000
1500
1000
500
0
****
****
BAL
Lung Homogenate
PBS
Mitoquinol, 10µg
Mitoquinol, 50µg

Figure 7

Supplementary Methods

Human Subjects

Study design and patient population. This study is an analysis of prospectively collected data from 39 subjects recruited from an ICU cohort from New York Presbyterian Hospital-Weill Cornell Medical Center (NYP-WMC). Subjects were recruited on the first or second day of their admission to the ICU. The cohort was derived from the Weill Cornell-Biobank of Critical Illness (WC-BOCI) at the NYP-WMC. Protocols for recruitment, data collection, and sample processing have been described previously [1-5]. Briefly, the WC-BOCI cohort recruited any patient admitted to the medical ICU, with exclusion for the lack of the ability to provide or the lack of a surrogate to provide informed consent and moribund state.

Clinical evaluation. Clinical and laboratory data were collected from the electronic health records by trained research personnel, with clinical adjudication of the final diagnosis of viral infection was confirmed by critical care board-certified attending physicians and clinical respiratory viral PCR (BioFire FilmArray RP2, BioFire Diagnostics, Salt Lake City, UT) was used to confirm viral etiology. ICU subjects without a concern for infection or in whom infection was not thought to be the cause of the current admission were used as the control population. Organ failure was defined by the SOFA scoring system, which quantifies the presence and severity of organ failure in 6 different organ systems [6].

Mice

Young adult (2 months) and aged adult (18 months) male and female BALB/c mice were purchased from the NIA rodent facility (Charles River Laboratories). Upon receipt, mice were handled under identical husbandry conditions and fed certified commercial feed. Body weights were measured daily and mice were humanely euthanized if they lost more than 15% of their

starting body weight. The IACUC at Weill Cornell Medicine approved the use of animals in this study and methods were carried out in accordance with the relevant guidelines and regulations. No animals were used in the study if there was evidence of skin lesions, weight loss, or lymphadenopathy.

Influenza (A/Puerto Rico/8/1934, H1N1)

Influenza viral stock (material #: 10100374, batch #: 4XP170531, EID_{50} per ml: $10^{10.3}$) was purchased from Charles River (Norwich, CT). $TCID_{50}$ was calculated using the Viral ToxGlo Assay (Promega, Madison WI). Briefly, BAL was diluted in 3.16-fold serial dilutions and plated for 24-48 hours on >80% confluent MDCK cells. Upon visualization of cytopathic effect, ATP detection reagent was added, and luminescence was measured. Values were calculated by plotting net relative luminescence units (RLU) values after subtracting average blank wells against viral dilution. The TCID50 value is the reciprocal of the dilution that produced a 50% decline in ATP levels compared to untreated controls. Validated regression analysis was performed using GraphPad Prism.

***In vivo* procedures and tissue collection**

Influenza infection: All mice were anesthetized with isoflurane (5% for induction and 2% for maintenance) prior to intranasal instillation with 12 PFU of influenza (50μL volume in PBS). Mitoquinol administration: Mice received a 100μL volume of PBS (vehicle) or 10-50μg dose of mitoquinol (Cayman Chemical) intraperitoneally starting at day 3 post influenza. BMS-986205 administration: Starting at day 0, mice received a daily intraperitoneal injection containing PBS or BMS-986205 (200μM) (Selleck Chemicals). Bronchoalveolar lavage (BAL): BAL was collected using previously published methods [7]. Briefly, 0.8-ml of PBS was slowly injected and aspirated 4 times prior to saving the recovered lavage fluid on ice. Lavage was clarified at 7000

rpm for 10 minutes at 4°C. Lung tissue collection: At select time points of infection lung tissue was collected from control and influenza infected young and aged adult mice. Tissue was snap frozen or placed into Allprotect (Qiagen) for future analysis. FITC-Dextran Lung Permeability Assay: Young and aged adult mice were intranasally instilled with 50-μL of FITC-Dextran (3mg/kg). After 1 hour, blood was collected from euthanized mice, and plasma was isolated after centrifugation (7000 rpm, 10 minutes). Fluorescence was assessed (excitation 485, emission 528). Lung Wet to Dry Ratio: Lung tissue was collected from control and influenza infected young and aged adult mice. Lung tissue weight was assessed at harvest (wet weight) and after being placed in a 60°C drying over for 48 hours (dry weight). Histology: Mice were euthanized, and right lung tissue was collected for downstream analysis. To maintain architecture, left lung was distended with 1% low melting agarose and placed into cold formalin [8]. Tissue samples were processed, and H&E stained by the Translational Research Program at WCM Pathology and Laboratory of Medicine. Images were scanned using the EVOS FL Auto Imaging System (ThermoFisher Scientific). For all animal experiments, we used 10 mice per group and experiments were repeated at least three times.

Primary bone marrow and alveolar macrophage isolation.

Bone marrow cells (BMCs) were prepared from the femurs and tibias of mice as previously described [9-11]. Alveolar macrophages were isolated from uninfected and influenza infected mice (day 3, 5, and 7) post instillation. Briefly, mice were lavaged with 5 x 1-ml of sterile PBS. Cells were collected and quantified.

***In vitro* cell culture treatments and assays.**

Bone marrow derived macrophages (BMM) were cultured with media alone or media containing LPS (Catalog #: tlrl-eblps, 100ng/ml) or poly I:C (HMW) (Catalog #: tlrl-pic, 1μg/ml) for 2, 4, or

24 hours (Invivogen, San Diego, CA). Aged BMM were treated with mitoTEMPO L (50μM) (Catalog #: 18796, Cayman Chemical), Trolox (50μM) (Catalog #: S3665, Selleck Chemicals, Houston TX), or mitoquinol (50μM) at time of plating (24h prior to stimulation). Young BMM were pre-treated with BMS-986205 (1μM) (Catalog #: S8629), NLG919 (1μM) (Catalog #: S7111), IDO inhibitor 1 (1μM) (Catalog #: S8557), Indoximod (1μM) (Catalog #: S7756) purchased from Selleck Chemicals) or 1-methyl-D_1-L-tryptophan (1μM) (Catalog #: ALX-106-040-M050, Enzo Life Sciences) 24 hours prior to stimulation. Young BMM were transfected with control or IDO1 specific siRNA (FlexiTube Gene Solution, Catalog #: GS15930, Qiagen) using GenMute siRNA transfection reagent for primary macrophages (Catalog #: SL100568-PMG, SignaGen Laboratories).

IDO1 specific activity assay

IDO1 specific activity was assessed using a standardized protocol (Catalog #: 9157-AO, R&D systems). Briefly, a substrate mixture (dilute ascorbic acid 80mM pH 8.0 mixed with 800μM L-tryptophan, 9000 units/mL catalase, and 40μM methylene blue in 50mM MES pH 6.5). Dilute rmIDO (8ng/μL) was used as a positive control. The reaction was started by adding 50μL of substrate mixture to 50μL of substrate blank, positive control, or sample and absorbance at 321 nm was measured and IDO1 specific activity was calculated: Specific Activity (pmol/min/mg) = [Adjusted V_{max} (OD/min) X well volume (L) x 10^{12} pmol/mol] / [extinction coefficient (3750 M^{-1} cm^{-1}) x pathway correction 0.32 cm x IDO1 concentration (μg)]. To confirm these results, samples were also assessed by fluorescence using the IDO1 enzyme assay kit (Catalog #: K972, Biovision).

Flow cytometry

Mitochondrial superoxide generation was detected using MitoSOX red indicator (Catalog #: M36008, ThermoFisher Scientific). Cells were loaded with 1ml of 5 μM MitoSOX and incubated for 10 minutes at 37°C. Cells were washed and analyzed. All samples were run on a BD Accuri and analyzed by Flow Jo software (Tree Star Inc., Ashland, OR).

NAD^+ Assay

Lung tissue was collected from control and influenza infected young and aged adult BALB/c and NAD^+ levels were assessed using the NAD/NADH Quantitation Colorimetric Kit (Biovision, Catalog# K337).

ELISA

Culture supernatants, lung homogenates, and BAL were analyzed for IL1β, IL10, TNFα, and IL6 production using ELISA kits purchased from Thermo Fisher Scientific. Kynurenine levels were measured by ELISA (Catalog #: E4629, BioVision) and repeated with sample acylation and detection (Catalog #: ISE-2227, Immusmol, Bordeaux, France). Tryptophan was quantified by fluorometric assessment (Catalog #: K557, BioVision) and repeated with precipitation and derivation prior to ELISA detection (Catalog #: ISE-2227, Immusmol). Protein levels were calculated using the BioRad protein assay (BioRad) per manufacturer's instructions.

$CD4^+CD25^+$ Cell Isolation

Lung tissue was homogenized using a glass dounce homogenizer to form single-cell suspensions prior to isolation using the EasySep Mouse $CD4^+CD25^+$ Regulatory T Cell Isolation Kit II (Catalog #: 18783, STEMCELL Technologies). $CD4^+$ T cells were first enriched by negative selection using the mouse $CD4^+$ T cell isolation cocktail followed by positive selection for $CD25^+$ T cells. Cells were stained with trypan blue and enumerated.

Metabolite Sample Accessioning: Following receipt, samples were inventoried and immediately stored at -80^{o}C. Each sample received was accessioned into the Metabolon LIMS system and was assigned by the LIMS a unique identifier that was associated with the original source identifier only. This identifier was used to track all sample handling, tasks, results, etc. The samples (and all derived aliquots) were tracked by the LIMS system. All portions of any sample were automatically assigned their own unique identifiers by the LIMS when a new task was created; the relationship of these samples was also tracked. All samples were maintained at -80^{o}C until processed.

Metabolite Sample Preparation: Samples were prepared using the automated MicroLab STAR® system from Hamilton Company. Several recovery standards were added prior to the first step in the extraction process for QC purposes. To remove protein, dissociate small molecules bound to protein or trapped in the precipitated protein matrix, and to recover chemically diverse metabolites, proteins were precipitated with methanol under vigorous shaking for 2 min (Glen Mills GenoGrinder 2000) followed by centrifugation. The resulting extract was divided into five fractions: two for analysis by two separate reverse phase (RP)/UPLC-MS/MS methods with positive ion mode electrospray ionization (ESI), one for analysis by RP/UPLC-MS/MS with negative ion mode ESI, one for analysis by HILIC/UPLC-MS/MS with negative ion mode ESI, and one sample was reserved for backup. Samples were placed briefly on a TurboVap® (Zymark) to remove the organic solvent. The sample extracts were stored overnight under nitrogen before preparation for analysis. Several types of controls were analyzed in concert with the experimental samples: a pooled matrix sample generated by taking a small volume of each experimental sample (or alternatively, use of a pool of well-characterized human plasma) served as a technical replicate throughout the data set; extracted water samples served as process blanks; and a cocktail of QC standards that were carefully

chosen not to interfere with the measurement of endogenous compounds were spiked into every analyzed sample, allowed instrument performance monitoring and aided chromatographic alignment. Instrument variability was determined by calculating the median relative standard deviation (RSD) for the standards that were added to each sample prior to injection into the mass spectrometers. Overall process variability was determined by calculating the median RSD for all endogenous metabolites (i.e., non-instrument standards) present in 100% of the pooled matrix samples. Experimental samples were randomized across the platform run with QC samples spaced evenly among the injections. Peaks were quantified using area-under-the-curve. A data normalization step was performed to correct variation resulting from instrument inter-day tuning differences. Essentially, each compound was corrected in run-day blocks by registering the medians to equal one (1.00) and normalizing each data point proportionately. In certain instances, biochemical data may have been normalized to an additional factor (e.g., cell counts, total protein as determined by Bradford assay, osmolality, etc.) to account for differences in metabolite levels due to differences in the amount of material present in each sample.

Ultrahigh Performance Liquid Chromatography-Tandem Mass Spectroscopy (UPLC-MS/MS): All methods utilized a Waters ACQUITY ultra-performance liquid chromatography (UPLC) and a Thermo Scientific Q-Exactive high resolution/accurate mass spectrometer interfaced with a heated electrospray ionization (HESI-II) source and Orbitrap mass analyzer operated at 35,000 mass resolution. The sample extract was dried then reconstituted in solvents compatible to each of the four methods. Each reconstitution solvent contained a series of standards at fixed concentrations to ensure injection and chromatographic consistency. One aliquot was analyzed using acidic positive ion conditions, chromatographically optimized for more hydrophilic compounds. In this method, the extract was gradient eluted from a C18 column (Waters UPLC BEH C18-2.1x100 mm, 1.7 µm) using water and methanol, containing 0.05%

perfluoropentanoic acid (PFPA) and 0.1% formic acid (FA). Another aliquot was also analyzed using acidic positive ion conditions, however it was chromatographically optimized for more hydrophobic compounds. In this method, the extract was gradient eluted from the same afore mentioned C18 column using methanol, acetonitrile, water, 0.05% PFPA and 0.01% FA and was operated at an overall higher organic content. Another aliquot was analyzed using basic negative ion optimized conditions using a separate dedicated C18 column. The basic extracts were gradient eluted from the column using methanol and water, however with 6.5mM Ammonium Bicarbonate at pH 8. The fourth aliquot was analyzed via negative ionization following elution from a HILIC column (Waters UPLC BEH Amide 2.1x150 mm, 1.7 µm) using a gradient consisting of water and acetonitrile with 10mM Ammonium Formate, pH 10.8. The MS analysis alternated between MS and data-dependent MS^n scans using dynamic exclusion. The scan range varied slighted between methods but covered 70-1000 m/z.

Bioinformatics: The informatics system consisted of four major components, the Laboratory Information Management System (LIMS), the data extraction and peak-identification software, data processing tools for QC and compound identification, and a collection of information interpretation and visualization tools for use by data analysts. The hardware and software foundations for these informatics components were the LAN backbone, and a database server running Oracle 10.2.0.1 Enterprise Edition.

Metabolite Quantification and Data Normalization: Peaks were quantified using area-under-the-curve. For studies spanning multiple days, a data normalization step was performed to correct variation resulting from instrument inter-day tuning differences. Following log transformation and imputation of missing values, if any, with the minimum observed value for each compound, Welch's two-sample t-test was used to identify biochemicals that differed significantly between experimental groups. Biochemicals that achieved statistical significance

($p \leq 0.05$) were presented. In additional, Spearman Correlation was used as a nonparametric measure of the strength and direction of association that exists between two variables.

Principal Components Analysis (PCA)

Principal components analysis is an unsupervised analysis that reduces the dimension of the data. Each principal component is a linear combination of every metabolite and the principal components are uncorrelated. The number of principal components is equal to the number of observations. The first principal component is computed by determining the coefficients of the metabolites that maximizes the variance of the linear combination. The second component finds the coefficients that maximize the variance with the condition that the second component is orthogonal to the first. The third component is orthogonal to the first two components and so on. The total variance is defined as the sum of the variances of the predicted values of each component (the variance is the square of the standard deviation), and for each component, the proportion of the total variance is computed.

RNA purification and real time PCR

RNA samples were extracted using the automated Maxwell RNA extraction protocol (Madison, WI). Samples were quantified and $A_{260/280}$ ratios were recorded. Samples were reverse transcribed using the First Stand Synthesis Kit and quantified using QuantiTect Primer Assays and RT^2 Profiler™ Assays (Mouse Mitochondria PAMM-0087Z) were used to assess gene expression (Qiagen). For Taqman assays, RNA was reverse transcribed using prior to assessment using Taqman Fast Advanced Master Mix and probes specific for metabolic genes (Mouse Amino Acid Metabolism, catalog #: 4391524) or genes associated with immune responses (Mouse Immune Response, catalog #: 4414079). All reactions were performed in triplicate. Relative levels of messenger RNA (mRNA) were calculated by the comparative cycle

threshold method and either β-Actin or β2M mRNA levels were used as the invariant control for each sample.

Statistical analysis: Murine Studies

Survival analysis between groups was calculated using the Mantel Cox test. Comparison of groups was performed using a two-tailed t-test and comparisons between groups were verified by one-way ANOVA. All samples were independent and contained the same sample size for analysis. All data were analyzed using GraphPad Prism software (San Diego, CA). Statistical significance was considered by a *P<0.05, **P<0.01, ***P<0.001, and ****P<0.0001.

Data availability

Most data generated during this study are included in this published article and its Supplementary Information files. The datasets generated during and/or analyzed during the current study are available from the corresponding author on reasonable request.

1. Ma KC, Schenck EJ, Siempos, II, Cloonan SM, Finkelsztein EJ, Pabon MA, Oromendia C, Ballman KV, Baron RM, Fredenburgh LE, Higuera A, Lee JY, Chung CR, Jeon K, Yang JH, Howrylak JA, Huh JW, Suh GY, Choi AM. Circulating RIPK3 levels are associated with mortality and organ failure during critical illness. *JCI Insight* 2018: 3(13).
2. Finkelsztein EJ, Jones DS, Ma KC, Pabon MA, Delgado T, Nakahira K, Arbo JE, Berlin DA, Schenck EJ, Choi AM, Siempos, II. Comparison of qSOFA and SIRS for predicting adverse outcomes of patients with suspicion of sepsis outside the intensive care unit. *Crit Care* 2017: 21(1): 73.
3. Dolinay T, Kim YS, Howrylak J, Hunninghake GM, An CH, Fredenburgh L, Massaro AF, Rogers A, Gazourian L, Nakahira K, Haspel JA, Landazury R, Eppanapally S, Christie JD, Meyer NJ, Ware LB, Christiani DC, Ryter SW, Baron RM, Choi AM. Inflammasome-regulated cytokines are critical mediators of acute lung injury. *Am J Respir Crit Care Med* 2012: 185(11): 1225-1234.
4. Park J, Pabon M, Choi AMK, Siempos, II, Fredenburgh LE, Baron RM, Jeon K, Chung CR, Yang JH, Park CM, Suh GY. Plasma surfactant protein-D as a diagnostic biomarker for acute respiratory distress syndrome: validation in US and Korean cohorts. *BMC Pulm Med* 2017: 17(1): 204.
5. Schenck EJ, Ma KC, Price DR, Nicholson T, Oromendia C, Gentzler ER, Sanchez E, Baron RM, Fredenburgh LE, Huh JW, Siempos, II, Choi AM. Circulating cell death biomarker TRAIL is associated with increased organ dysfunction in sepsis. *JCI Insight* 2019: 4(9).
6. Vincent JL, Moreno R, Takala J, Willatts S, De Mendonca A, Bruining H, Reinhart CK, Suter PM, Thijs LG. The SOFA (Sepsis-related Organ Failure Assessment) score to describe organ dysfunction/failure. On behalf of the Working Group on Sepsis-Related Problems of the European Society of Intensive Care Medicine. *Intensive Care Med* 1996: 22(7): 707-710.
7. Sun F, Xiao G, Qu Z. Murine Bronchoalveolar Lavage. *Bio Protoc* 2017: 7(10).
8. Halbower AC, Mason RJ, Abman SH, Tuder RM. Agarose infiltration improves morphology of cryostat sections of lung. *Lab Invest* 1994: 71(1): 149-153.
9. Inaba K, Inaba M, Romani N, Aya H, Deguchi M, Ikehara S, Muramatsu S, Steinman RM. Generation of large numbers of dendritic cells from mouse bone marrow cultures supplemented with granulocyte/macrophage colony-stimulating factor. *The Journal of experimental medicine* 1992: 176(6): 1693-1702.
10. Zhang X, Goncalves R, Mosser DM. The isolation and characterization of murine macrophages. *Current protocols in immunology / edited by John E Coligan [et al]* 2008: Chapter 14: Unit 14 11.
11. Cho SJ, Rooney K, Choi AMK, Stout-Delgado HW. NLRP3 inflammasome activation in aged macrophages is diminished during Streptococcus pneumoniae infection. *Am J Physiol Lung Cell Mol Physiol* 2018: 314(3): L372-L387.
12. Misharin AV, Morales-Nebreda L, Mutlu GM, Budinger GR, Perlman H. Flow cytometric analysis of macrophages and dendritic cell subsets in the mouse lung. *Am J Respir Cell Mol Biol* 2013: 49(4): 503-510.

Supplemental Captions

Supplemental Table 1 (related to Figure 6): Metabolic gene expression in young and aged murine lung and alveolar macrophages during influenza infection.

Supplemental Table 2 (related to Figure 6): Mitochondrial gene expression in young and aged murine lung during influenza infection.

Supplemental Figure 1 (related to Figure 2): (A) Correlation of kynurenine and tryptophan levels in severe influenza patients by age. (B) Weight change and (C) survival during influenza infection.

Supplemental Figure 2 (related to Figure 5): IL6 production by young bone marrow derived macrophages in response to IDO1 modulators and co-stimulation with (A) LPS or (B) poly I:C. (C) IDO1 expression and (D) specific activity was assessed in young macrophages post treatment with IDO1 inhibitor BMS-986205. Comparison of IL6 production post (E) LPS or (F) poly I:C stimulation of untreated or IDO1 inhibited young macrophages. Student's t-test: **P<0.01, ***P<0.001, and ****P<0.0001. Similar results were obtained from at least three independent experiments with N=10 per group. Data are expressed as the mean $\pm$ SD.

Supplemental Figure 3 (related to Figure 6): Aged bone marrow derived macrophages were pre-treated with antioxidants prior to stimulation with LPS. (A) IL6 production was measured at 4- and 24-hours post stimulation. (B) Impact of mitoquinol (50μM) on IDO1 expression was assessed in response to 24-hour stimulation with LPS or poly I:C. (C) Ratio of kynurenine to tryptophan in response to mitoquinol was measured in aged macrophages at 4- and 24-hours post stimulation. Student's t-test: ***P<0.001 and ****P<0.0001. Similar results were obtained

from at least three independent experiments with N=10 per group. Data are expressed as the mean ± SD.

Supplemental Figure 4 (related to Figure 7): (A) Schematic overview of mitoquinol administration in aged mice. (B) Weight change was assessed in PBS or mitoquinol controls (solid circle and square, respectively) and compared to influenza infected treated with PBS (solid up triangle, black line) or mitoquinol (solid down triangle, blue line). (C) Viral titers were measured in BAL collected on day 7 (Q50: mitoquinol, 50μM). (D) BAL cells were collected from young, aged, and aged + mitoquinol (50μM) treated mice during the course of influenza infection and strained with mitoSOX. Fluorescence was assessed by flow cytometry. Student's t-test: ***P<0.001 and ****P<0.0001. Similar results were obtained from at least three independent experiments with N=10 per group. Data are expressed as the mean ± SD.

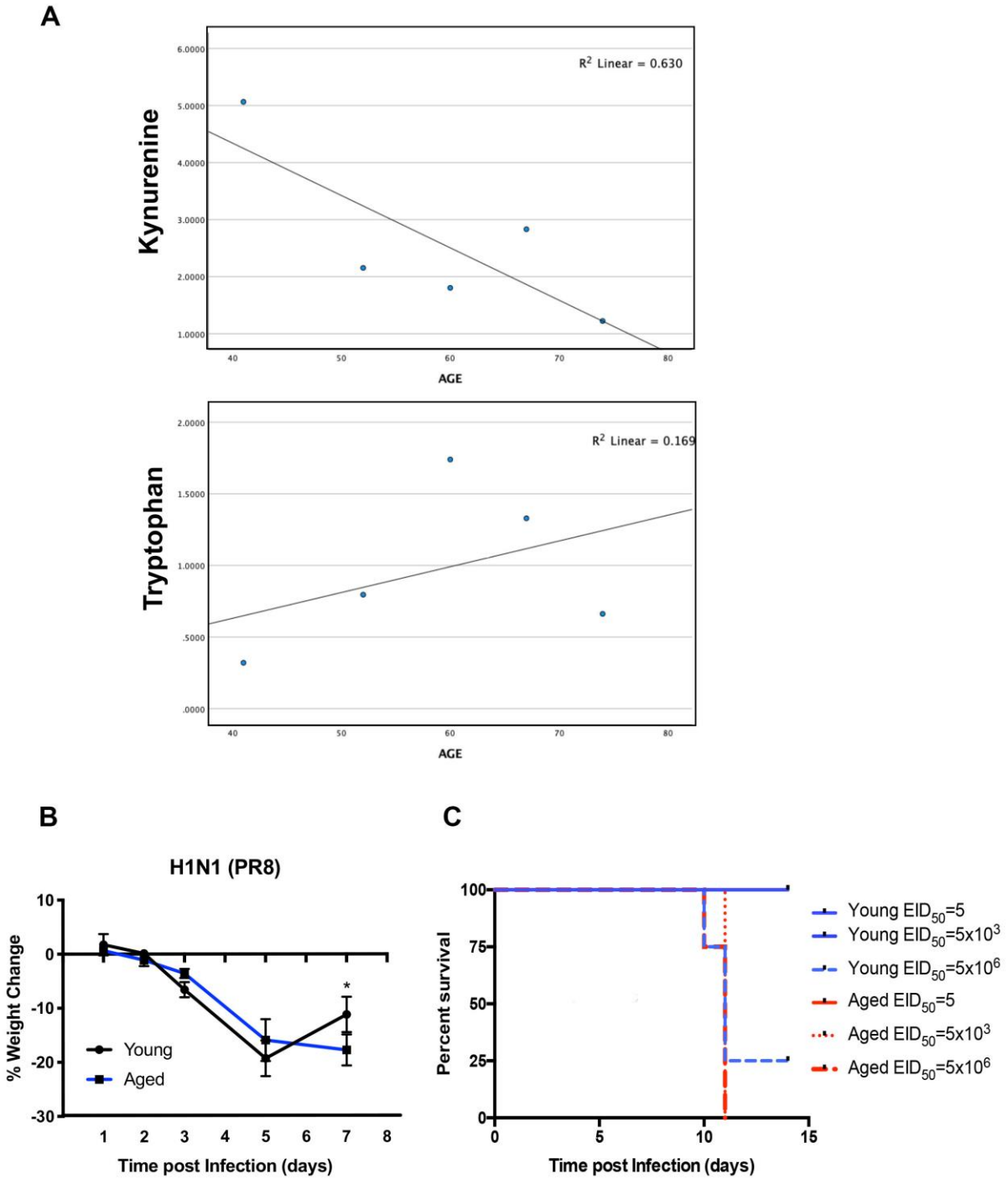

Supplemental Figure 1

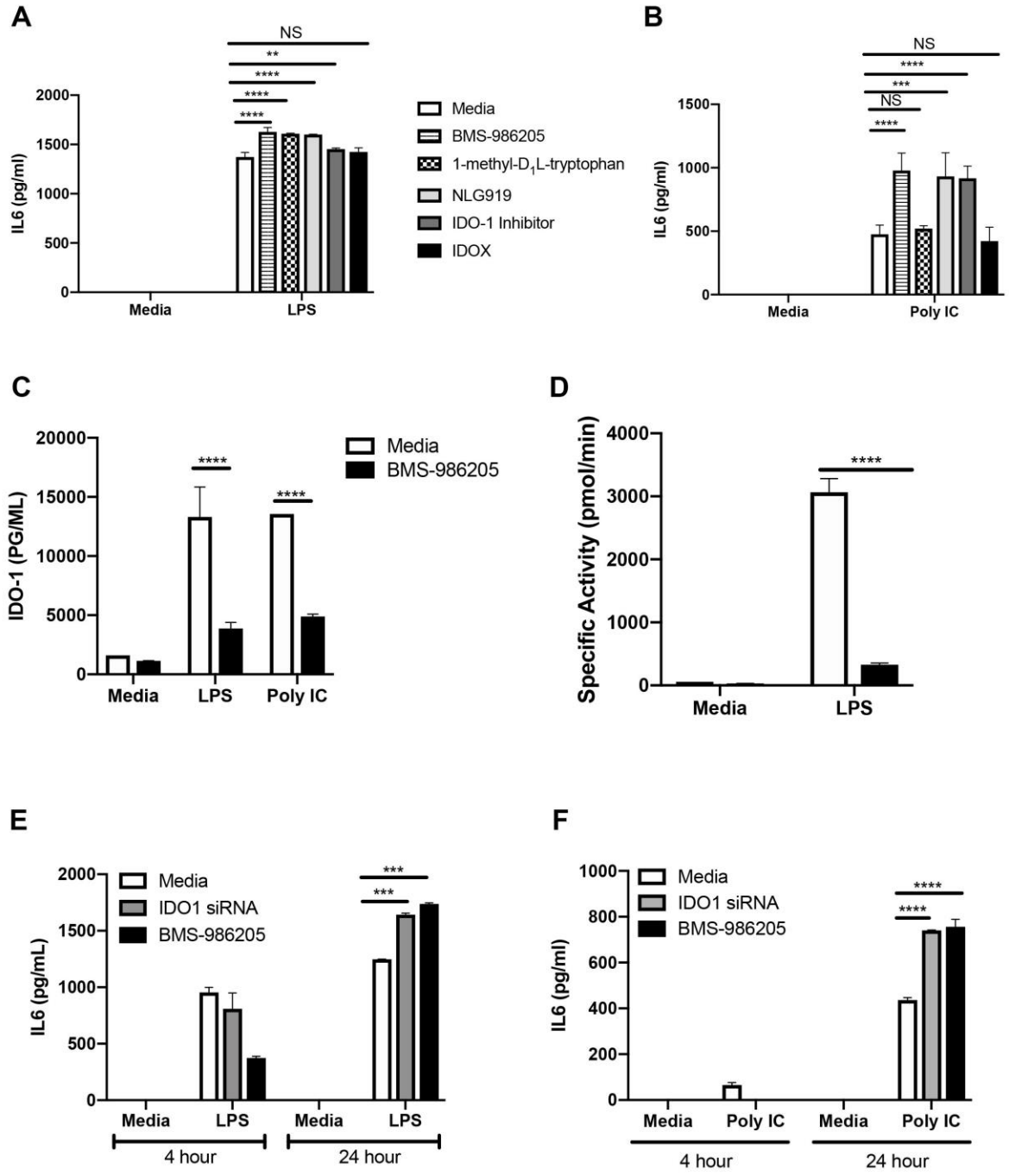

Supplemental Figure 2

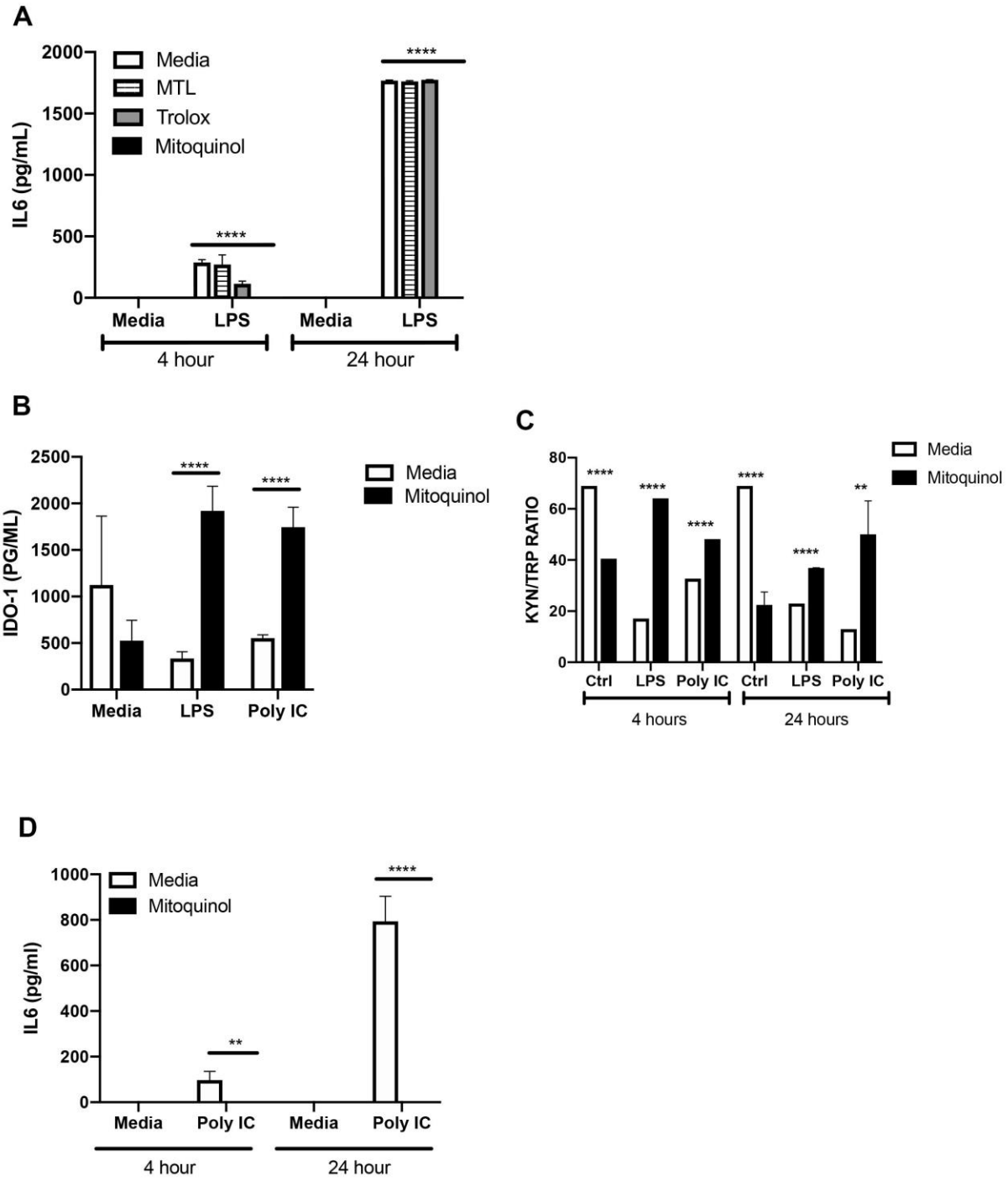

Supplemental Figure 3

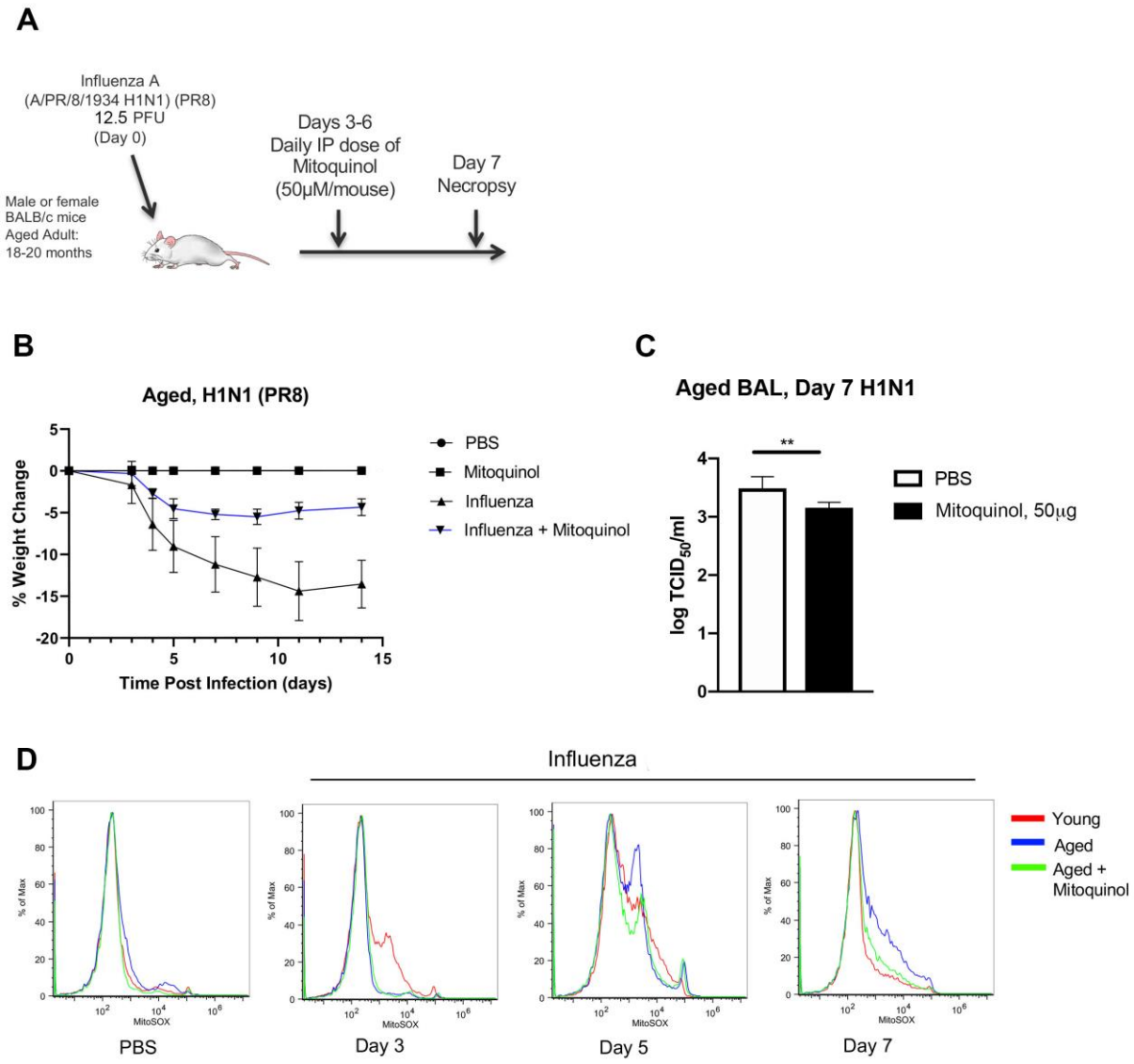

Supplemental Figure 4

Figure 6A, Lung Tissue	Gene Symbol	Expression Level (Relative to Age Matched Control)	Standard Deviation	Comparison	p-value	Comparison	p-value
Young Lung, Day 3	*Ahcy*	0.5894	0.2371				
Young Lung, Day 3	*Bhmt*	5.2983	2.6844				
Young Lung, Day 3	*Ido1*	45.1913	16.6326				
Young Lung, Day 3	*Oxct2a*	6.4512	3.4155				
Young Lung, Day 3	*Srm*	0.7590	0.0805				
Young Lung, Day 3	*Tph2*	18.8481	4.8577				
Young Lung, Day 5	*Ahcy*	0.7000	0.3254	vs YD3	0.6591		
Young Lung, Day 5	*Bhmt*	6.6731	5.8717	vs YD3	0.731		
Young Lung, Day 5	*Ido1*	66.4320	10.7966	vs YD3	0.1371		
Young Lung, Day 5	*Oxct2a*	11.7513	2.7486	vs YD3	0.1044		
Young Lung, Day 5	*Srm*	0.6547	0.1002	vs YD3	0.2328		
Young Lung, Day 5	*Tph2*	7.2443	2.0209	vs YD3	0.0188		
Young Lung, Day 7	*Ahcy*	0.4358	0.2548	vs YD5	0.3304		
Young Lung, Day 7	*Bhmt*	0.9010	0.7660	vs YD5	0.1666		
Young Lung, Day 7	*Ido1*	147.8444	30.3462	vs YD5	0.003		
Young Lung, Day 7	*Oxct2a*	3.8412	0.4350	vs YD5	0.0604		
Young Lung, Day 7	*Srm*	0.3426	0.0757	vs YD5	0.0126		
Young Lung, Day 7	*Tph2*	3.2862	0.9607	vs YD5	0.0375		
Aged Lung, Day 3	*Ahcy*	2.2994	0.0391	vs YD3	0.0002		
Aged Lung, Day 3	*Bhmt*	5.3009	1.4232	vs YD3	0.9989		
Aged Lung, Day 3	*Ido1*	6.9562	1.0443	vs YD3	0.0165		
Aged Lung, Day 3	*Oxct2a*	9.4775	1.5507	vs YD3	0.2348		
Aged Lung, Day 3	*Srm*	2.2025	0.5406	vs YD3	0.0102		
Aged Lung, Day 3	*Tph2*	7.5754	2.7806	vs YD3	0.0252		
Aged Lung, Day 5	*Ahcy*	16.8788	26.8847	vs YD5	0.3561	vs AD3	0.4008
Aged Lung, Day 5	*Bhmt*	128.1025	28.0884	vs YD5	0.3896	vs AD3	0.3847

Aged Lung, Day 5	*Ido1*	17.0251	0.3449	vs YD5	0.0014	vs AD3	<0.0001
Aged Lung, Day 5	*Oxct2a*	218.9703	20.7026	vs YD5	0.4072	vs AD3	0.3982
Aged Lung, Day 5	*Srm*	3.8886	4.8877	vs YD5	0.3158	vs AD3	0.5845
Aged Lung, Day 5	*Tph2*	10.4179	8.7654	vs YD5	0.5742	vs AD3	0.6208
Aged Lung, Day 7	*Ahcy*	74.7335	38.1660	vs YD7	0.028	vs AD5	0.0984
Aged Lung, Day 7	*Bhmt*	420.1965	178.2890	vs YD7	0.0152	vs AD5	0.1469
Aged Lung, Day 7	*Ido1*	31.8139	4.6891	vs YD7	0.0003	vs AD5	0.0055
Aged Lung, Day 7	*Oxct2a*	526.6681	141.6959	vs YD7	0.0031	vs AD5	0.0453
Aged Lung, Day 7	*Srm*	12.8656	7.1444	vs YD7	0.0386	vs AD5	0.1469
Aged Lung, Day 7	*Tph2*	15.0500	2.5880	vs YD7	0.0018	vs AD5	0.4294

Supplemental Table 1 (related to Figure 6): Metabolic gene expression in young and aged murine lung and alveolar macrophages during influenza infection.

Sample	Gene Symbol	Accession Number	Fold Regulation (Comparing to Young Control Group)	Standard Deviation	p-value
Aged Control	*Dnm1*	NM_152816	1.58	0.234245	<.00001
Aged Control	*Uxt*	NM_013840	9.39	0.234245	<.00001
Aged Control	*Lrpprc*	NM_028233	13.68	0.008263	<.00001
Aged Control	*Msto1*	NM_144898	66.73	0.007589	<.00001
Aged Control	*Rhot1*	NM_021536	-207.69	0.00823	<.00001
Aged Control	*Opa1*	NM_133752	-3.14	0.031803	<.00001
Aged Control	*Nefl*	NM_010910	61.63	0.018787	<.00001
Aged Control	*Rhot2*	NM_145999	3.48	0.013376	<.00001
Aged Control	*Fis1*	NM_025562	-5.13	0.019065	<.00001
Aged Control	*Cox10*	NM_178379	17.27	0.003446	<.00001
Aged Control	*Timm23*	NM_016897	1.39	0.004842	<.00001
Aged Control	*Timm44*	NM_011592	-1.04	0.00398	<.00001
Aged Control	*Timm10*	NM_013899	8.39	0.023751	<.00001
Aged Control	*Timm50*	NM_025616	1.85	0.044106	<.00001
Aged Control	*Immp1l*	NM_028260	-1.19	0.034824	<.00001
Aged Control	*Timm17a*	NM_011590	1.53	0.028881	<.00001
Aged Control	*Immp2l*	NM_053122	1.18	0.234245	<.00001
Aged Control	*Timm8b*	NM_013897	2.99	0.095470	<.00001
Aged Control	*Timm22*	NM_019818	14.38	0.047256	<.00001
Aged Control	*Timm8a1*	NM_013898	17.41	0.063537	<.00001
Aged Control	*Timm9*	NM_001024853	3.87	0.002554	<.00001
Aged Control	*Taz*	NM_181516	2.48	0.028792	<.00001
Aged Control	*Timm17b*	NM_011591	10.11	0.014457	<.00001
Aged Control	*Tspo*	NM_009775	1.28	0.234245	<.00001
Aged Control	*Aip*	NM_016666	-326.34	0.003166	<.00001
Aged Control	*Hspd1*	NM_010477	-90.97	0.054196	<.00001
Aged Control	*Mipep*	NM_027436	-64.85	0.013615	<.00001
Aged Control	*Dnajc19*	NM_026332	12.4	0.061241	<.00001
Aged Control	*Grpel1*	NM_024478	2.33	0.012067	<.00001
Aged Control	*Bak1*	NM_007523	-161	0.178643	<.00001
Aged Control	*Ucp2*	NM_011671	-6.6	0.024373	<.00001
Aged Control	*Bcl2l1*	NM_009743	3.53	0.014027	<.00001
Aged Control	*Stard3*	NM_021547	2.65	0.031873	<.00001
Aged Control	*Ucp3*	NM_009464	7.6	0.108464	<.00001
Aged Control	*Mtx2*	NM_016804	-5.55	0.020456	<.00001
Aged Control	*Trp53*	NM_011640	1.74	0.069787	<.00001
Aged Control	*Bcl2*	NM_009741	8.67	0.010395	<.00001
Aged Control	*Cpt2*	NM_009949	34.97	0.034522	<.00001
Aged Control	*Bnip3*	NM_009760	3.02	0.028107	<.00001
Aged Control	*Ucp1*	NM_009463	271.99	0.027232	<.00001

Sample	Gene Symbol	Accession Number	Fold Regulation (Comparing to Age-Matched Control Group)	Standard Deviation	p-value
Young, Day 3	*Dnm1*	NM_152816	-1.21	0.276608	0.022
Young, Day 3	*Uxt*	NM_013840	1.11	0.136816	0.325
Young, Day 3	*Lrpprc*	NM_028233	-1.67	0.206227	<.00001
Young, Day 3	*Msto1*	NM_144898	-1.52	0.257993	0.0015
Young, Day 3	*Rhot1*	NM_021536	-1.81	0.411938	<.00001
Young, Day 3	*Opa1*	NM_133752	-1.93	0.176302	0.0098
Young, Day 3	*Nefl*	NM_010910	-16.03	0.464787	<.00001
Young, Day 3	*Rhot2*	NM_145999	-1.41	0.088974	0.0383
Young, Day 3	*Fis1*	NM_025562	-1.24	0.294903	0.004282
Young, Day 3	*Cox10*	NM_178379	-1.41	0.278589	0.03421
Young, Day 3	*Timm23*	NM_016897	-1.16	0.046935	0.1079
Young, Day 3	*Timm44*	NM_011592	-1.3	0.048469	<.00001
Young, Day 3	*Timm10*	NM_013899	-1.01	0.134599	0.962442
Young, Day 3	*Timm50*	NM_025616	-1.32	0.096663	0.001482
Young, Day 3	*Immp1l*	NM_028260	-1.16	0.252645	0.312214
Young, Day 3	*Timm17a*	NM_011590	-1.5	0.229514	0.006123
Young, Day 3	*Immp2l*	NM_053122	-1.14	0.258759	0.5616
Young, Day 3	*Timm8b*	NM_013897	-1.13	0.125470	0.615718
Young, Day 3	*Timm22*	NM_019818	-1.4	0.312279	<.00001
Young, Day 3	*Timm8a1*	NM_013898	1.02	0.407620	0.775596
Young, Day 3	*Timm9*	NM_001024853	-1.24	0.034566	0.357806
Young, Day 3	*Taz*	NM_181516	-1.96	0.106519	0.00106
Young, Day 3	*Timm17b*	NM_011591	-1.24	0.227383	0.053124
Young, Day 3	*Tspo*	NM_009775	2.02	0.081228	0.006535
Young, Day 3	*Aip*	NM_016666	-1.2	0.148237	0.025979
Young, Day 3	*Hspd1*	NM_010477	-1.33	0.263548	0.003565
Young, Day 3	*Mipep*	NM_027436	-1.52	0.478993	0.000322
Young, Day 3	*Dnajc19*	NM_026332	-1.35	0.450200	<.00001
Young, Day 3	*Grpel1*	NM_024478	-1.3	0.214436	0.033441
Young, Day 3	*Bak1*	NM_007523	1.91	0.179809	0.018645
Young, Day 3	*Ucp2*	NM_011671	1.15	0.339305	0.429549
Young, Day 3	*Bcl2l1*	NM_009743	1.8	0.270009	0.052695
Young, Day 3	*Stard3*	NM_021547	1.18	0.132324	0.028373
Young, Day 3	*Ucp3*	NM_009464	-1.82	0.342365	0.149324
Young, Day 3	*Mtx2*	NM_016804	-1.39	0.136178	0.020888
Young, Day 3	*Trp53*	NM_011640	-1.18	0.349259	0.008851
Young, Day 3	*Bcl2*	NM_009741	-1.34	0.376117	0.038421
Young, Day 3	*Cpt2*	NM_009949	-1.3	0.404090	<.00001
Young, Day 3	*Bnip3*	NM_009760	-1.8	0.046847	0.019592
Young, Day 3	*Ucp1*	NM_009463	-1.27	0.146030	0.184052
Young, Day 5	*Dnm1*	NM_152816	1.42	0.504624	<.00001

Young, Day 5	*Uxt*	NM_013840	12.65	0.504624	0.03981
Young, Day 5	*Lrpprc*	NM_028233	11.49	0.245218	<.00001
Young, Day 5	*Msto1*	NM_144898	62.02	0.129610	0.011003
Young, Day 5	*Rhot1*	NM_021536	-59.82	0.049236	<.00001
Young, Day 5	*Opa1*	NM_133752	-1.55	0.118029	0.041582
Young, Day 5	*Nefl*	NM_010910	71.88	0.080253	<.00001
Young, Day 5	*Rhot2*	NM_145999	2.71	0.265818	<.00001
Young, Day 5	*Fis1*	NM_025562	-1.94	0.416093	0.005582
Young, Day 5	*Cox10*	NM_178379	7.75	0.136866	0.007912
Young, Day 5	*Timm23*	NM_016897	1.29	0.334353	0.003668
Young, Day 5	*Timm44*	NM_011592	-1.63	0.425082	0.002017
Young, Day 5	*Timm10*	NM_013899	8.09	0.063743	<.00001
Young, Day 5	*Timm50*	NM_025616	1.37	0.450599	0.002651
Young, Day 5	*Immp1l*	NM_028260	-1.6	0.203274	0.002205
Young, Day 5	*Timm17a*	NM_011590	1.2	0.192552	0.024196
Young, Day 5	*Immp2l*	NM_053122	-1.06	0.504624	0.784423
Young, Day 5	*Timm8b*	NM_013897	2.14	0.010644	0.058192
Young, Day 5	*Timm22*	NM_019818	-1.52	0.194743	0.0068
Young, Day 5	*Timm8a1*	NM_013898	26.9	0.351398	0.04255
Young, Day 5	*Timm9*	NM_001024853	3.17	0.110566	0.0003
Young, Day 5	*Taz*	NM_181516	1.61	0.560437	<.00001
Young, Day 5	*Timm17b*	NM_011591	5.57	0.419023	<.00001
Young, Day 5	*Tspo*	NM_009775	1.35	0.144071	<.00001
Young, Day 5	*Aip*	NM_016666	-211.05	0.567809	<.00001
Young, Day 5	*Hspd1*	NM_010477	-119.66	0.591613	<.00001
Young, Day 5	*Mipep*	NM_027436	-32.97	0.238810	<.00001
Young, Day 5	*Dnajc19*	NM_026332	10.28	0.452715	0.006514
Young, Day 5	*Grpel1*	NM_024478	1.04	0.437263	0.621469
Young, Day 5	*Bak1*	NM_007523	-104.12	0.649544	<.00001
Young, Day 5	*Ucp2*	NM_011671	-8.05	0.007086	<.00001
Young, Day 5	*Bcl2l1*	NM_009743	2.3	0.395370	<.00001
Young, Day 5	*Stard3*	NM_021547	1.06	0.092171	0.645164
Young, Day 5	*Ucp3*	NM_009464	9.21	0.567306	0.006138
Young, Day 5	*Mtx2*	NM_016804	-7.21	0.195900	<.00001
Young, Day 5	*Trp53*	NM_011640	1.65	0.496157	0.021792
Young, Day 5	*Bcl2*	NM_009741	6.36	0.542077	<.00001
Young, Day 5	*Cpt2*	NM_009949	13.05	0.088991	0.002113
Young, Day 5	*Bnip3*	NM_009760	3.32	0.149408	<.00001
Young, Day 5	*Ucp1*	NM_009463	9.21	0.168199	0.006138
Young, Day 7	*Dnm1*	NM_152816	1.05	0.597455	0.035165
Young, Day 7	*Uxt*	NM_013840	6.13	1.066828	0.005907
Young, Day 7	*Lrpprc*	NM_028233	7.14	0.109391	<.00001
Young, Day 7	*Msto1*	NM_144898	32.86	0.037669	0.005234
Young, Day 7	*Rhot1*	NM_021536	-156.09	0.270979	<.00001
Young, Day 7	*Opa1*	NM_133752	-3.8	0.188513	<.00001
Young, Day 7	*Nefl*	NM_010910	35.64	0.077665	<.00001
Young, Day 7	*Rhot2*	NM_145999	1.59	0.241696	0.00136
Young, Day 7	*Fis1*	NM_025562	-5.22	0.150909	<.00001
Young, Day 7	*Cox10*	NM_178379	9.06	0.235001	<.00001

Young, Day 7	*Timm23*	NM_016897	-1.49	0.377833	<.00001
Young, Day 7	*Timm44*	NM_011592	-2.37	0.235430	<.00001
Young, Day 7	*Timm10*	NM_013899	4.84	0.025478	<.00001
Young, Day 7	*Timm50*	NM_025616	-1	0.210938	0.979085
Young, Day 7	*Immp1l*	NM_028260	-2.93	0.157736	<.00001
Young, Day 7	*Timm17a*	NM_011590	1.25	0.210426	0.164741
Young, Day 7	*Immp2l*	NM_053122	-2	0.597455	<.00001
Young, Day 7	*Timm8b*	NM_013897	1.53	0.537806	0.053186
Young, Day 7	*Timm22*	NM_019818	6.71	0.328362	0.0339
Young, Day 7	*Timm8a1*	NM_013898	10.02	0.083040	0.013729
Young, Day 7	*Timm9*	NM_001024853	2.05	0.129774	<.00001
Young, Day 7	*Taz*	NM_181516	1.33	0.176826	0.000401
Young, Day 7	*Timm17b*	NM_011591	3.84	0.334999	<.00001
Young, Day 7	*Tspo*	NM_009775	-1.04	0.188223	0.18011
Young, Day 7	*Aip*	NM_016666	-538.53	0.444077	<.00001
Young, Day 7	*Hspd1*	NM_010477	-210.73	0.467772	<.00001
Young, Day 7	*Mipep*	NM_027436	-86.83	0.201459	<.00001
Young, Day 7	*Dnajc19*	NM_026332	5.32	0.143707	0.000945
Young, Day 7	*Grpel1*	NM_024478	-5.66	0.519921	<.00001
Young, Day 7	*Bak1*	NM_007523	-349.18	0.462343	<.00001
Young, Day 7	*Ucp2*	NM_011671	-8.99	0.113515	<.00001
Young, Day 7	*Bcl2l1*	NM_009743	1.94	0.180355	0.010866
Young, Day 7	*Stard3*	NM_021547	1.31	0.213277	0.000647
Young, Day 7	*Ucp3*	NM_009464	4.26	0.131223	0.000518
Young, Day 7	*Mtx2*	NM_016804	-27.05	0.249469	<.00001
Young, Day 7	*Trp53*	NM_011640	-1.61	0.202487	0.001181
Young, Day 7	*Bcl2*	NM_009741	5.38	0.482395	<.00001
Young, Day 7	*Cpt2*	NM_009949	14.54	0.122620	0.003356
Young, Day 7	*Bnip3*	NM_009760	2.24	0.118614	<.00001
Young, Day 7	*Ucp1*	NM_009463	175.36	0.151104	<.00001
Aged, Day 3	*Dnm1*	NM_152816	1.55	0.009084	0.043715
Aged, Day 3	*Uxt*	NM_013840	11.24	0.008823	0.15646
Aged, Day 3	*Lrpprc*	NM_028233	15.4	0.069221	0.00436
Aged, Day 3	*Msto1*	NM_144898	74.84	0.040968	0.002063
Aged, Day 3	*Rhot1*	NM_021536	-27.81	0.009290	<.00001
Aged, Day 3	*Opa1*	NM_133752	-2.39	0.009989	0.009518
Aged, Day 3	*Nefl*	NM_010910	72.55	0.011790	<.00001
Aged, Day 3	*Rhot2*	NM_145999	3.56	0.015750	<.00001
Aged, Day 3	*Fis1*	NM_025562	-2.23	0.022224	0.001792
Aged, Day 3	*Cox10*	NM_178379	10.99	0.014878	<.00001
Aged, Day 3	*Timm23*	NM_016897	1.56	0.015046	0.001236
Aged, Day 3	*Timm44*	NM_011592	-1.49	0.011485	0.000632
Aged, Day 3	*Timm10*	NM_013899	9.17	0.002329	0.00416
Aged, Day 3	*Timm50*	NM_025616	2.5	0.034689	0.072834
Aged, Day 3	*Immp1l*	NM_028260	1.04	0.023079	0.714177
Aged, Day 3	*Timm17a*	NM_011590	1.37	0.018242	0.176057
Aged, Day 3	*Immp2l*	NM_053122	1.97	0.029655	0.077852
Aged, Day 3	*Timm8b*	NM_013897	2.7	0.009976	0.002277
Aged, Day 3	*Timm22*	NM_019818	21.59	0.003378	0.015706

Aged, Day 3	*Timm8a1*	NM_013898	24	0.023224	0.005406
Aged, Day 3	*Timm9*	NM_001024853	2.65	0.041939	0.000884
Aged, Day 3	*Taz*	NM_181516	1.94	0.035182	0.011774
Aged, Day 3	*Timm17b*	NM_011591	5.65	0.014351	<.00001
Aged, Day 3	*Tspo*	NM_009775	1.7	0.015642	0.012537
Aged, Day 3	*Aip*	NM_016666	-42.52	0.039833	<.00001
Aged, Day 3	*Hspd1*	NM_010477	-27.8	0.057325	<.00001
Aged, Day 3	*Mipep*	NM_027436	-8.45	0.034962	0.001985
Aged, Day 3	*Dnajc19*	NM_026332	11.05	0.025641	0.004137
Aged, Day 3	*Grpel1*	NM_024478	2.74	0.033677	0.04677
Aged, Day 3	*Bak1*	NM_007523	-20.98	0.024509	<.00001
Aged, Day 3	*Ucp2*	NM_011671	-6.04	0.081806	<.00001
Aged, Day 3	*Bcl2l1*	NM_009743	2.77	0.040080	0.004991
Aged, Day 3	*Stard3*	NM_021547	1.97	0.024514	0.103553
Aged, Day 3	*Ucp3*	NM_009464	9.94	0.033115	0.002557
Aged, Day 3	*Mtx2*	NM_016804	-9.18	0.025300	<.00001
Aged, Day 3	*Trp53*	NM_011640	2.45	0.044229	0.141116
Aged, Day 3	*Bcl2*	NM_009741	7.55	0.008663	0.000132
Aged, Day 3	*Cpt2*	NM_009949	24	0.021854	0.037972
Aged, Day 3	*Bnip3*	NM_009760	3.48	0.036900	0.014444
Aged, Day 3	*Ucp1*	NM_009463	341.22	0.020438	0.004431
Aged, Day 5	*Dnm1*	NM_152816	-1.01	0.146542	0.911012
Aged, Day 5	*Uxt*	NM_013840	6.33	0.095936	0.02311
Aged, Day 5	*Lrpprc*	NM_028233	7.73	0.500106	0.022061
Aged, Day 5	*Msto1*	NM_144898	32.86	0.245397	0.038452
Aged, Day 5	*Rhot1*	NM_021536	-27.45	0.079576	0.030487
Aged, Day 5	*Opa1*	NM_133752	-2.29	0.186770	0.945039
Aged, Day 5	*Nefl*	NM_010910	51.56	0.256888	0.000145
Aged, Day 5	*Rhot2*	NM_145999	2.15	0.233226	0.000215
Aged, Day 5	*Fis1*	NM_025562	-2.55	0.985528	0.084987
Aged, Day 5	*Cox10*	NM_178379	9.84	0.169465	0.003546
Aged, Day 5	*Timm23*	NM_016897	-1.25	0.346803	0.203831
Aged, Day 5	*Timm44*	NM_011592	-1.77	0.048058	0.001601
Aged, Day 5	*Timm10*	NM_013899	7.5	0.315747	0.003268
Aged, Day 5	*Timm50*	NM_025616	1.39	0.108186	0.000517
Aged, Day 5	*Immp1l*	NM_028260	-1.14	0.272310	0.886216
Aged, Day 5	*Timm17a*	NM_011590	1.31	0.200554	0.221618
Aged, Day 5	*Immp2l*	NM_053122	2.51	0.233891	0.325789
Aged, Day 5	*Timm8b*	NM_013897	2.81	0.200125	0.044259
Aged, Day 5	*Timm22*	NM_019818	12.33	0.089578	<.00001
Aged, Day 5	*Timm8a1*	NM_013898	14.97	0.186268	0.000224
Aged, Day 5	*Timm9*	NM_001024853	3.31	0.050286	0.03209
Aged, Day 5	*Taz*	NM_181516	1.55	0.087231	0.090484
Aged, Day 5	*Timm17b*	NM_011591	7.63	0.441561	0.002352
Aged, Day 5	*Tspo*	NM_009775	1	0.430336	0.924165
Aged, Day 5	*Aip*	NM_016666	-42.66	0.445553	0.059826
Aged, Day 5	*Hspd1*	NM_010477	-8.78	0.100013	0.266323
Aged, Day 5	*Mipep*	NM_027436	-6.09	0.164420	0.992009
Aged, Day 5	*Dnajc19*	NM_026332	9.03	0.037270	<.00001

Aged, Day 5	*Grpel1*	NM_024478	1.52	0.278815	0.050674
Aged, Day 5	*Bak1*	NM_007523	-27.01	0.170585	0.07297
Aged, Day 5	*Ucp2*	NM_011671	-6.03	0.257942	0.000204
Aged, Day 5	*Bcl2l1*	NM_009743	2.83	0.074613	<.00001
Aged, Day 5	*Stard3*	NM_021547	1.41	0.234839	0.031205
Aged, Day 5	*Ucp3*	NM_009464	9.83	0.309822	0.117646
Aged, Day 5	*Mtx2*	NM_016804	-3.67	0.426456	0.598652
Aged, Day 5	*Trp53*	NM_011640	2.55	0.845030	0.325059
Aged, Day 5	*Bcl2*	NM_009741	6.32	0.231227	<.00001
Aged, Day 5	*Cpt2*	NM_009949	13.88	0.118755	0.081
Aged, Day 5	*Bnip3*	NM_009760	2.46	0.136180	0.001122
Aged, Day 5	*Ucp1*	NM_009463	205.48	0.289786	<.00001
Aged, Day 7	*Dnm1*	NM_152816	-1.22	0.338499	0.00575
Aged, Day 7	*Uxt*	NM_013840	2.86	0.692317	<.00001
Aged, Day 7	*Lrpprc*	NM_028233	3.42	0.414982	0.00086
Aged, Day 7	*Msto1*	NM_144898	10.26	0.173457	0.004218
Aged, Day 7	*Rhot1*	NM_021536	-1.83	0.720092	0.000729
Aged, Day 7	*Opa1*	NM_133752	3.79	0.501125	0.007413
Aged, Day 7	*Nefl*	NM_010910	126.73	0.355153	0.009879
Aged, Day 7	*Rhot2*	NM_145999	4.62	0.495839	<.00001
Aged, Day 7	*Fis1*	NM_025562	3.31	0.174977	0.110276
Aged, Day 7	*Cox10*	NM_178379	5.99	0.092679	0.014145
Aged, Day 7	*Timm23*	NM_016897	-1.51	0.319041	0.045507
Aged, Day 7	*Timm44*	NM_011592	-3.31	0.901894	<.00001
Aged, Day 7	*Timm10*	NM_013899	11.21	0.242170	0.001588
Aged, Day 7	*Timm50*	NM_025616	2.13	0.434837	0.00547
Aged, Day 7	*Immp1l*	NM_028260	2.2	0.028053	0.000214
Aged, Day 7	*Timm17a*	NM_011590	3.77	0.233049	0.033529
Aged, Day 7	*Immp2l*	NM_053122	33.81	0.117738	0.008799
Aged, Day 7	*Timm8b*	NM_013897	8.34	0.100017	<.00001
Aged, Day 7	*Timm22*	NM_019818	10.67	1.234722	<.00001
Aged, Day 7	*Timm8a1*	NM_013898	21.26	0.089677	<.00001
Aged, Day 7	*Timm9*	NM_001024853	2.02	0.215694	0.000161
Aged, Day 7	*Taz*	NM_181516	1.39	0.095744	0.036774
Aged, Day 7	*Timm17b*	NM_011591	2.7	0.833042	0.001452
Aged, Day 7	*Tspo*	NM_009775	-1.09	0.514886	0.206547
Aged, Day 7	*Aip*	NM_016666	-1.14	0.142870	0.003014
Aged, Day 7	*Hspd1*	NM_010477	1.98	0.120963	<.00001
Aged, Day 7	*Mipep*	NM_027436	4.49	0.231783	<.00001
Aged, Day 7	*Dnajc19*	NM_026332	9.87	0.231839	<.00001
Aged, Day 7	*Grpel1*	NM_024478	2.15	0.175277	0.016379
Aged, Day 7	*Bak1*	NM_007523	1.34	0.087229	0.001697
Aged, Day 7	*Ucp2*	NM_011671	-1.9	0.516107	0.031873
Aged, Day 7	*Bcl2l1*	NM_009743	4.05	0.290585	0.003837
Aged, Day 7	*Stard3*	NM_021547	4.03	0.039858	0.000727
Aged, Day 7	*Ucp3*	NM_009464	19.72	0.273746	0.000654
Aged, Day 7	*Mtx2*	NM_016804	4.18	0.157227	0.032098
Aged, Day 7	*Trp53*	NM_011640	25.98	0.473444	0.004285
Aged, Day 7	*Bcl2*	NM_009741	7.72	0.748018	0.010335

Aged, Day 7	*Cpt2*	NM_009949	6.8	0.116384	0.002479
Aged, Day 7	*Bnip3*	NM_009760	1.82	0.154687	0.015362
Aged, Day 7	*Ucp1*	NM_009463	190.17	0.349982	0.004236
Aged + Mitoquinol, Day 7	*Dnm1*	NM_152816	1.17	0.397769	0.23858
Aged + Mitoquinol, Day 7	*Uxt*	NM_013840	8.57	0.426294	<.00001
Aged + Mitoquinol, Day 7	*Lrpprc*	NM_028233	10.71	0.431704	0.009413
Aged + Mitoquinol, Day 7	*Msto1*	NM_144898	51.13	0.177585	0.004643
Aged + Mitoquinol, Day 7	*Rhot1*	NM_021536	-46.91	0.469786	<.00001
Aged + Mitoquinol, Day 7	*Opa1*	NM_133752	-3.29	0.32921	0.00186
Aged + Mitoquinol, Day 7	*Nefl*	NM_010910	52.67	0.308935	0.000618
Aged + Mitoquinol, Day 7	*Rhot2*	NM_145999	2.4	0.415887	0.043976
Aged + Mitoquinol, Day 7	*Fis1*	NM_025562	-3.81	0.267968	<.00001
Aged + Mitoquinol, Day 7	*Cox10*	NM_178379	11.52	0.139843	0.000224
Aged + Mitoquinol, Day 7	*Timm23*	NM_016897	-1.07	0.27862	0.755264
Aged + Mitoquinol, Day 7	*Timm44*	NM_011592	-1.62	0.582019	0.00012
Aged + Mitoquinol, Day 7	*Timm10*	NM_013899	6.85	0.413409	0.003886
Aged + Mitoquinol, Day 7	*Timm50*	NM_025616	1.39	0.048376	0.217671
Aged + Mitoquinol, Day 7	*Immp1l*	NM_028260	-1.64	0.048865	<.00001
Aged + Mitoquinol, Day 7	*Timm17a*	NM_011590	1.64	0.21643	0.026529
Aged + Mitoquinol, Day 7	*Immp2l*	NM_053122	2.44	0.312735	0.028918
Aged + Mitoquinol, Day 7	*Timm8b*	NM_013897	2.6	0.100162	0.008141
Aged + Mitoquinol, Day 7	*Timm22*	NM_019818	-1.07	0.674714	0.897246
Aged + Mitoquinol, Day 7	*Timm8a1*	NM_013898	16.95	0.042623	0.004286
Aged + Mitoquinol, Day 7	*Timm9*	NM_001024853	3.22	0.188356	0.024159
Aged + Mitoquinol, Day 7	*Taz*	NM_181516	1.78	0.037415	0.046644
Aged + Mitoquinol, Day 7	*Timm17b*	NM_011591	7.19	0.553259	0.005694
Aged + Mitoquinol, Day 7	*Tspo*	NM_009775	1.01	0.346962	0.840712
Aged + Mitoquinol, Day 7	*Aip*	NM_016666	-109.46	0.128616	<.00001
Aged + Mitoquinol, Day 7	*Hspd1*	NM_010477	-19.93	0.034826	<.00001
Aged + Mitoquinol, Day 7	*Mipep*	NM_027436	-9.01	0.114109	<.00001

Aged + Mitoquinol, Day 7	*Dnajc19*	NM_026332	9.3	0.090138	0.003655
Aged + Mitoquinol, Day 7	*Grpel1*	NM_024478	1.67	0.081456	0.255945
Aged + Mitoquinol, Day 7	*Bak1*	NM_007523	-97.99	0.021808	<.00001
Aged + Mitoquinol, Day 7	*Ucp2*	NM_011671	-8.34	0.180185	<.00001
Aged + Mitoquinol, Day 7	*Bcl2l1*	NM_009743	3.21	0.16866	0.006696
Aged + Mitoquinol, Day 7	*Stard3*	NM_021547	1.79	0.052062	0.076156
Aged + Mitoquinol, Day 7	*Ucp3*	NM_009464	6.71	0.084753	0.007286
Aged + Mitoquinol, Day 7	*Mtx2*	NM_016804	-7.42	0.076796	<.00001
Aged + Mitoquinol, Day 7	*Trp53*	NM_011640	1.84	0.184653	0.091384
Aged + Mitoquinol, Day 7	*Bcl2*	NM_009741	6.91	0.396556	0.001698
Aged + Mitoquinol, Day 7	*Cpt2*	NM_009949	32.19	0.152104	0.014784
Aged + Mitoquinol, Day 7	*Bnip3*	NM_009760	2.79	0.084317	0.0115
Aged + Mitoquinol, Day 7	*Ucp1*	NM_009463	240.05	0.28728	0.003394

Supplemental Table 2: Fold change in mitochondrial gene expression in young and aged murine lung during influenza infection.